International Journal of Pharmacology

Int. J. Pharmacol. **2026**; 22(7): 54720
https://doi.org/10.31083/IJP54720

Research Article

Paeoniae Radix Alba Treats Diarrhea-Predominant Irritable Bowel Syndrome Through Regulation of the AGE/RAGE/NF-κB Signaling Pathway

Pengfei Han[1,†], Yali Yuan[2,†], Fengqiang Wang[1], Weidong Wu[3], Jian Zhang[3,*]

[1]Department of Gastroenterology, Zhangjiakou First Hospital, 075000 Zhangjiakou, Hebei, China
[2]Department of Traditional Chinese Medicine, Hebei North University, 075000 Zhangjiakou, Hebei, China
[3]Department of Basic Medicine, Heilongjiang University of Chinese Medicine, 150040 Harbin, Heilongjiang, China
*Correspondence: 18845055805@163.com (Jian Zhang)
[†]These authors contributed equally.

Academic Editors: Mozaniel Santana de Oliveira and Mehmet Ozaslan
Submitted: 9 June 2026 Revised: 29 July 2026 Accepted: 5 August 2026 Published: 23 November 2026

Abstract

Background: This study aimed to investigate the effects of Paeoniae Radix Alba (PRA) on irritable bowel syndrome with diarrhea (IBS-D) and its potential molecular mechanisms. **Methods:** An IBS-D mouse model was established by intracolonic instillation of acetic acid combined with restraint and tail-clip stress. Mice were randomly assigned to blank, model, control, low-dose PRA (PRA-L), medium-dose PRA (PRA-M), high-dose PRA (PRA-H), receptor for advanced glycation end products (RAGE) inhibitor (FPS-ZM1), and PRA-H + FPS-ZM1 groups. After 14 days of continuous intervention, the general condition of the mice was observed. Hematoxylin–eosin (HE) staining and immunohistochemistry were used to evaluate intestinal histopathological changes and the expression of nuclear factor kappa B (NF-κB), RAGE, and TP53. Serum levels of inflammatory cytokines were measured by enzyme-linked immunosorbent assay (ELISA). The expression of molecules related to the advanced glycation end products (AGEs)/RAGE/NF-κB pathway and apoptosis was assessed by quantitative polymerase chain reaction (qPCR) and Western blot. Meanwhile, transcriptomics and network pharmacology were integrated to screen for key components, core targets, and pathways involved in PRA treatment of IBS-D. **Results:** The PRA fingerprint indicated that the samples contained paeoniflorin, with good reproducibility. Compared with the model group, PRA intervention improved food intake and body weight, reduced fecal water content and small intestinal transit rate, ameliorated intestinal mucosal structural damage, and restored expression of zonula occludens-1 (ZO-1), occludin, claudin-1, and mucin 2 (MUC2). Combined transcriptomic and network pharmacology analysis revealed that the core targets of PRA against IBS-D mainly included tumor necrosis factor (TNF), interleukin-6 (IL6), TP53, and inhibitor of nuclear factor kappa B kinase subunit beta (IKBKB), which were co-enriched in the AGE/RAGE, NF-κB, and apoptosis-related pathways. Animal experiments further confirmed that PRA markedly reduced the levels of inflammatory factors such as interleukin-6 (IL-6), tumor necrosis factor-alpha (TNF-α), interleukin-1 beta (IL-1β), monocyte chemoattractant protein-1 (MCP-1), and endothelin-1 (EDN1); downregulated the mRNA expression of *Rage*, *Ikbkb*, *Nfkb*, *Il6*, and *Tnf*; inhibited RAGE, IKBKB, and p-p65/p65 protein expression; decreased the expression of TP53, Bcl-2-associated X protein (Bax), and cleaved caspase-3; increased B-cell lymphoma 2 (Bcl-2) levels; reduced the number of terminal deoxynucleotidyl transferase dUTP nick end labeling (TUNEL)-positive cells. The combination of PRA and FPS-ZM1 showed greater effects than either agent alone. **Conclusions:** PRA significantly ameliorates the diarrheal phenotype, intestinal mucosal inflammation, barrier dysfunction, and tissue apoptosis in mice with IBS-D. These effects appear to be mediated by inhibition of the AGE/RAGE/NF-κB signaling pathway.

Keywords: Paeoniae Radix Alba; diarrhea-type irritable bowel syndrome; immune inflammation; apoptosis; RAGE/NF-κB pathway

1. Introduction

Among functional disorders of the gut-brain axis, irritable bowel syndrome (IBS) stands out as the most frequently encountered condition, distinguished by chronically relapsing abdominal discomfort coupled with abnormal defecation habits [1,2,3]. Based on stool characteristics, four clinical subtypes have been delineated: IBS with predominant diarrhea (IBS-D), IBS with predominant constipation, mixed-type IBS, and unclassified IBS. IBS-D accounts for the largest share of clinical cases and is principally characterized by frequent loose stools, abdominal cramping, heightened bowel movement frequency, and an urgent need to defecate, all of which severely erode patients' quality of life and daily productivity [4,5,6]. Global prevalence estimates place IBS at approximately 10–11%, with IBS-D carrying a disproportionately heavy clinical burden given its persistent diarrheal course, prolonged duration, and tendency toward recurrence [7]. Although classified as non-life-threatening, the chronic and oscillating nature of IBS-D is frequently accompanied by psychological comorbidities—including anxiety, depression, disturbed sleep, and chronic pain—along with escalated healthcare expenditures, reflecting the intricate interplay among gastrointestinal, neurological, immune, and

Copyright: © 2026 The Author(s). Published by IMR Press.
This is an open access article under the CC BY 4.0 license.

Publisher's Note: IMR Press stays neutral with regard to jurisdictional claims in published maps and institutional affiliations.

endocrine systems that underlies this condition [8]. The origins of IBS-D are multifactorial, spanning genetic susceptibility, dietary triggers, post-infectious sequelae, and psychosocial stress. Key pathogenic mechanisms include dysregulated gut-brain communication, heightened visceral pain sensitivity, disordered gastrointestinal motility, low-grade mucosal inflammation, weakened epithelial barrier function, bile acid malabsorption, and compositional shifts in intestinal microbiota [9,10]. Among these, increased epithelial permeability, mucosal immune activation, and altered microbial metabolic output are increasingly regarded as central drivers of persistent diarrheal symptoms [11,12,13]. Current management strategies for IBS-D encompass dietary modification, antispasmodics, antidiarrheal agents, rifaximin, probiotics, neuromodulatory drugs, and cognitive-behavioral therapies [14,15]. However, these interventions are largely symptomatic in nature and fail to address the underlying pathophysiological drivers, resulting in inconsistent therapeutic responses and suboptimal long-term outcomes for many patients [16,17]. Consequently, there is a pressing need to identify therapeutic agents capable of simultaneously engaging multiple pathological targets while maintaining favorable safety profiles.

Paeoniae Radix Alba (PRA), prepared from the desiccated roots of Paeonia lactiflora Pall. (family Paeoniaceae), contains a rich repertoire of pharmacologically active compounds, with monoterpene glycosides, flavonoids, tannins, and volatile oils representing the major chemical categories. Among these, monoterpene glycosides—exemplified by paeoniflorin—are the most characteristic constituents and form the cornerstone of PRA's pharmacological activity [18,19]. Extensive research has documented that PRA and its bioactive molecules exhibit a broad spectrum of biological effects, encompassing analgesic, antispasmodic, anti-inflammatory, antioxidant, immunomodulatory, neuroprotective, and gastrointestinal barrier-protective properties [20]. Specifically, paeoniflorin has been shown to attenuate pain signaling through suppression of transient receptor potential vanilloid 1 (TRPV1) and its downstream inflammatory cascades, and to counteract lipopolysaccharide (LPS)-induced disruption of intestinal epithelial integrity and associated inflammatory responses [21]. Furthermore, PRA has demonstrated considerable promise in addressing gastrointestinal disorders and stress-related pathologies through its ability to reshape gut microbiota composition, dampen intestinal inflammation, and modulate emotion-regulating neural circuits [22].

Notwithstanding the therapeutic promise of PRA for IBS, earlier studies have predominantly focused on single bioactive compounds or isolated signaling pathways, leaving the global mechanism of action insufficiently characterized. To bridge this gap, the present investigation employs an integrated approach combining transcriptomic profiling with network pharmacology to systematically unravel the molecular mechanisms through which PRA exerts its therapeutic effects on IBS. This strategy is designed to establish a mechanistic framework for understanding the pharmacological material basis of PRA, inform precision-based traditional Chinese medicine interventions for IBS, and facilitate the development of novel therapeutics derived from this botanical source.

2. Materials and Methods

2.1 Construction of Animal Models

Eighty male C57BL/6 mice (8 weeks of age, 21 ± 3 g) were procured from Liaoning Changsheng Biotechnology Co., Ltd. (SCXK-2025-0001, Benxi, Liaoning, China) and maintained under specific pathogen-free conditions (22 ± 2 °C, 50–60% relative humidity, 12-h light/dark cycle) with unrestricted access to standard rodent chow and water. The IBS-D model was established through a comprehensive protocol (acetic acid colon perfusion combined with restraint and tail clamping stress) over a period of 21 consecutive days; not all animals treated with this protocol exhibited IBS-D-like phenotypes. To ensure that only mice with confirmed IBS-D-like phenotypes assessed by body weight, fecal moisture content ([(wet weight – dry weight) / wet weight] × 100%), intestinal transit speed (Transit rate (%) = (distance traveled by Evans blue/total small intestinal length) × 100%), and small intestine length were included in the treatment stage, we verified the successful construction of the model before random grouping. This approach aims to reduce inter-individual differences caused by the inconsistency of the model establishment process, thereby enhancing the statistical power and interpretability of the therapeutic effect [23].

2.2 Grouping and Administration

Following successful model induction, mice were randomized into eight groups (n = 10 per group) via a random number table: blank, model, control, Paeoniae Radix Alba low dose (PRA-L), Paeoniae Radix Alba medium dose (PRA-M), Paeoniae Radix Alba high dose (PRA-H), receptor for advanced glycation end product (RAGE) inhibitor (FPS-ZM1), and PRA-H + FPS-ZM1. For aqueous extract preparation, 20 g of PRA material was combined with a 10-fold volume of distilled water, soaked for 30 min, and subjected to two successive extractions at 100 °C. The combined extracts were concentrated to 1.04 g/mL and stored at 4 °C. PRA-L, PRA-M, and PRA-H groups received oral gavage of 2.6, 5.2, and 10.4 g/kg PRA extract, respectively. Dose levels were derived from preliminary dose-finding experiments and extrapolated from clinical adult dosages using body surface area conversion: the low dose approximated the clinical equivalent, while medium and high doses represented 2-fold and 4-fold multiples thereof. The control group received 19.47 mg/kg pinaverium bromide (PBT) (Abbott, batch No: 731133, Bangkok, Thailand) via oral gavage, converted from the clinical regimen (50 mg per dose, three times daily) via body surface area

scaling. FPS-ZM1 (Abcam, batch No: Ab235552, Cambridge, UK) was injected intraperitoneally at 1 mg/kg. The combination group received both 10.4 g/kg PRA (oral gavage) and 1 mg/kg FPS-ZM1 (intraperitoneal) simultaneously. All treatments were given once daily for 14 consecutive days. The study protocol was approved by the Animal Experiment Ethics Committee of Heilongjiang University of Chinese Medicine (SYXK-202605012) and adhered to the Animal Research: Reporting of *In Vivo* Experiments (ARRIVE) guidelines [24]. At the end of the intervention, mice were anesthetized using 1% sodium pentobarbital (Sigma-Aldrich, batch No: Y0002194, St. Louis, Missouri, USA) administered at 50 mg/kg via intraperitoneal injection. Blood was collected from the abdominal aorta into non-anticoagulant tubes, allowed to clot at room temperature for 30 min, and centrifuged at 3000 rpm for 10 min at 4 °C. The separated serum was aliquoted and stored at –80 °C. Animals were then euthanized by cervical dislocation. Distal colon tissue was promptly harvested, rinsed with ice-cold saline to remove luminal contents, and divided: one segment was fixed in 4% paraformaldehyde (Beyotime, batch No: P0099, Shanghai, China) for histological assessment, while the other was flash-frozen in liquid nitrogen and stored at –80 °C for subsequent molecular analyses.

2.3 Establishment of HPLC Fingerprints

PRA was obtained from the the First Affiliated Hospital of Heilongjiang University of Chinese Medicine, and taxonomically verified by Professor Huifeng Sun. For sample preparation, 0.1 g of finely ground PRA powder was transferred to a 50 mL volumetric flask, dissolved in 35 mL of 50% ethanol, and subjected to ultrasonic extraction for 30 min. The resulting solution was passed through a membrane filter to yield the test sample. A paeoniflorin reference standard (Shifeng, batch No: C18355195, Shanghai, China) was prepared at 0.1 mg/mL in methanol as the reference solution. Chromatographic separation was achieved on a C18 analytical column (2.1 mm × 100 mm, 1.7 µm particle size) using a gradient elution program with acetonitrile and 0.05% aqueous phosphoric acid as the mobile phase, delivered at 0.4 mL/min. Detection was performed at 230 nm with column temperature held at 30 °C, injection volume of 2 µL, and total run time of 70 min. The high performance liquid chromatography (HPLC) fingerprint was established by computing relative retention times and relative peak areas of characteristic peaks normalized to the paeoniflorin reference peak. Paeoniflorin identity was confirmed by comparing its retention time with that of the authentic standard (tolerance <0.05 min) and by matching ultraviolet (UV) absorption profiles at 230 nm. Similarity assessment was carried out using the Similarity Evaluation System for Chromatographic Fingerprint of Traditional Chinese Medicine (Version 2012, Chinese Pharmacopoeia Commission, Beijing, China). Common peaks were defined as those consistently detected across all replicate injections, with relative retention times calculated against the paeoniflorin reference. Replicate chromatogram similarity indices were computed to assess batch-to-batch consistency. Integration parameters were set as follows: peak width threshold of 0.1 min, slope sensitivity of 50, and minimum peak area of 0.05 mAU·min. These parameters ensure analytical reproducibility and scientific interpretability of the fingerprint.

2.4 Transcriptomics and Network Pharmacology

Control, model and PRA-H group consisted of 6 distal colon tissue samples were collected and total RNA was isolated using TRIzol reagent (Thermo Fisher Scientific, batch No: 15596018CN, Waltham, Massachusetts, USA). RNA quantity and quality were assessed on a NanoDrop spectrophotometer (Thermo Fisher Scientific, Model No: 840-317500, USA), while RNA integrity was evaluated with an Agilent Bioanalyzer (Agilent Technologies, Model No: 2100, Santa Clara, California, USA). Sequencing libraries were constructed from 2 µg of total RNA using the NEBNext Ultra II RNA Library Prep Kit for Illumina, involving poly(A) mRNA enrichment, fragmentation, double-stranded cDNA synthesis, end repair, A-tailing, and adapter ligation. cDNA fragments of ~500 bp were size-selected with AMPure XP beads (Beckman Coulter, batch No: A63881, Indianapolis, Indiana, USA), followed by PCR amplification and purification. Library quality was validated on the Agilent 2100 Bioanalyzer, and after qPCR quantification, paired-end sequencing (PE150) was performed on an Illumina platform. Clean reads were mapped to the reference genome with HISAT2 (v2.1.0) (https://daehwankimlab.github.io/hisat2/), gene-level read counts were computed via HTSeq (v0.9.1) (https://htseq.readthedocs.io/en/latest/), and expression levels were normalized using the Fragments Per Kilobase of transcript per Million mapped reads (FPKM) method. Differentially expressed gene (DEG) screening and weighted gene co-expression network analysis (WGCNA) were carried out with thresholds of $|\log2FoldChange| > 1$ and $p < 0.05$. Gene Ontology (GO) and Kyoto Encyclopedia of Genes and Genomes (KEGG) pathway enrichment analyses were executed using topGO and KEGG tools, respectively, with $p < 0.05$ as the significance threshold.

Bioactive constituents of PRA were mined from the Traditional Chinese Medicine Systems Pharmacology Database and Analysis Platform (TCMSP; https://www.tcmsp-e.com/), applying dual inclusion thresholds of oral bioavailability (OB) ≥30% and drug-likeness (DL) ≥0.18. Putative protein targets of each candidate compound were subsequently assembled. Disease-associated targets for IBS were compiled from the GeneCards (https://www.genecards.org/) and SymMap (http://www.symmap.org/) repositories. The Venny 2.1.0 tool (https://bioinfogp.cnb.csic.es/tools/venny/) was used to identify the intersection between compound-associated and disease-associated target

sets. Visualization of the compound-target interaction network was performed in Cytoscape 3.9.1 (https://cytoscape.org/), where nodes exhibiting the highest degree centrality were designated as core bioactive compounds. A protein-protein interaction (PPI) network for the shared targets was constructed through the STRING database (Homo sapiens; confidence threshold >0.9). For integration with the transcriptomic data, DEGs identified from mouse tissues were mapped to their human orthologs using the Mouse Genome Informatics (MGI) homology database and the Ensembl BioMart ortholog mapping tool. Only genes with confirmed one-to-one orthologous relationships between mouse and human were retained for cross-referencing. Functional annotation encompassing GO terms across biological process (BP), cellular component (CC), and molecular function (MF) domains, together with KEGG pathway enrichment, was carried out via the DAVID database ($p < 0.05$). Molecular docking simulations between top 5 compounds including kaempferol, benzoyl paeoniflorin, lactiflorin, paeoniflorin, albiflorin, and key target proteins including AKT serine/threonine kinase 1 (AKT1) (PDB ID: 6HHF), interleukin 6 (IL6) (PDB ID: 1ALU), tumor necrosis factor (TNF) (PDB ID: 2AZ5), B-cell lymphoma 2 (BCL2) (PDB ID: 6FBX), signal transducer and activator of transcription 3 (STAT3) (PDB ID: 6NJS) were conducted using AutoDock Vina (https://vina.scripps.edu/), with binding affinities below –5.0 kcal·mol^{-1} considered indicative of favorable interactions. Docking poses were rendered using PyMOL (https://pymol.org/). This analytical workflow enabled systematic prediction of the principal active compounds, pivotal molecular targets, and candidate signaling cascades potentially mediating the therapeutic effects of PRA against IBS.

2.5 Enzyme-Linked Immunosorbent Assay (ELISA)

Serum specimens were collected from mice in all experimental groups. Concentrations of inflammatory cytokines and related markers—interleukin-6 (IL-6), tumor necrosis factor-alpha (TNF-α), interleukin-1 beta (IL-1β), monocyte chemoattractant protein-1 (MCP-1), nuclear factor kappa B (NF-κB), endothelin-1 (EDN1) (Meimian, batch No: 14206, 920, 12681, 29628, 14307, 0648, China) were quantified using commercial ELISA kits following the manufacturers' recommended protocols. Absorbance was measured at 450 nm on a microplate reader (Thermo Fisher Scientific, Model No: VLBL00GD2, USA), and analyte concentrations were calculated from corresponding standard curves.

2.6 Histopathological Evaluation

2.6.1 Hematoxylin-Eosin (HE) Staining

Fixed distal colon tissue was immersed in 4% paraformaldehyde for 24 h, then processed through standard dehydration, clearing, paraffin infiltration, and embedding. Sections of approximately 4 μm thickness were prepared on a paraffin microtome, mounted on glass slides, and dried at 37 °C for 12 h. Following dewaxing in xylene and rehydration through a graded ethanol series (100%, 95%, 90%, 80%, 70%), sections were stained with hematoxylin and eosin (Solarbio, batch No: C0105S, Beijing, China) and examined under light microscopy. Histological assessment employed a semi-quantitative scoring system: villus height and crypt depth were quantified using ImageJ (https://imagej.net/); epithelial damage was graded (0 = normal, 1 = mild irregularity, 2 = moderate damage with focal necrosis, 3 = severe destruction); inflammatory cell infiltration was scored (0 = none, 1 = mild, 2 = moderate, 3 = severe). Five non-overlapping fields per section were randomly selected at 200× magnification, and mean scores were calculated.

2.6.2 Immunohistochemistry

Following deparaffinization and rehydration, antigen retrieval was performed by incubating sections in ethylenediaminetetraacetic acid (EDTA) buffer for 30 min. Endogenous peroxidase was quenched with 3% hydrogen peroxide for 1 h at room temperature, followed by blocking of non-specific binding with normal goat serum for 1 h. Sections were then incubated overnight at 4 °C with primary antibodies against NF-κB (1:500) and TP53 (1:500) (Abcam, batch No: ab32536, ab238071, UK) in a humidified chamber. The following day, sections were equilibrated to room temperature, washed three times with PBS (5 min each), and incubated with species-matched secondary antibodies (Beyotime, batch No: A0208, China) for 2 h, followed by 3,3′-diaminobenzidine (DAB) chromogen development (Beyotime, batch No: P0202, China). Nuclei were counterstained with hematoxylin, and sections were dehydrated, cleared, and mounted. Positive staining was visualized microscopically and quantified using ImageJ. For immunohistochemistry (IHC) quantification, five non-overlapping fields per section were randomly selected at 200× magnification. The positively stained area was measured using ImageJ software with a uniform color threshold applied across all images. The percentage of positive area relative to total tissue area was calculated. Analysis was performed by two independent observers in a blinded fashion to minimize subjective bias, and results were averaged.

2.6.3 Immunofluorescence

Following deparaffinization, rehydration, and antigen retrieval using standard procedures, tissue sections were incubated with blocking buffer for 30 min at room temperature. Sections were then exposed to primary antibodies against RAGE (1:500) and NF-κB (1:500) (Abcam, batch No: ab216329, ab32536, UK) overnight at 4 °C under light-protected conditions. The next day, after equilibrating to room temperature, sections were extensively washed and subsequently incubated with fluorophore-conjugated secondary antibodies for 2 h at room temper-

ature in the dark. Following additional washes, nuclei were visualized by counterstaining with 4′,6-diamidino-2-phenylindole (DAPI) (Beyotime, batch No: C1006, China). An anti-fade mounting medium (Beyotime, batch No: P0126, China) was applied, and sections were coverslipped and examined under a fluorescence microscope with image acquisition. Positive area (%) = (positively stained area / total tissue area) × 100%.

2.6.4 TUNEL Assay

After PBS washing, sections were permeabilized by incubation with Proteinase K solution (Beyotime, Batch No: ST535, China) (final concentration: 40 µg/mL) for 30 min at 37 °C, followed by three PBS washes. Terminal deoxynucleotidyl transferase dUTP nick end labeling (TUNEL) reaction mixture (Beyotime, Batch No: C1086, China) was freshly prepared, and 50 µL was applied to each tissue section. Sections were incubated for 1 h at 37 °C in the dark. Following removal of the reaction mixture, sections were washed twice with PBS and then subjected to three 5-min washes in 0.1% Triton X-100 (Beyotime, Batch No: ST1723, China) solution supplemented with 5 mg/mL bovine serum albumin (BSA) (Sigma-Aldrich, Batch No: 10711454001, St. Louis, Missouri, USA). DAPI staining solution (5 µg/mL) was applied for 5 min at room temperature in the dark for nuclear counterstaining. After final PBS washes, anti-fade mounting medium was applied, and sections were immediately examined and photographed under a fluorescence microscope. Apoptotic index (%) = (TUNEL-positive cells / total DAPI-positive cells) × 100%.

2.7 Real-Time Quantitative Polymerase Chain Reaction Detection

Total RNA was extracted from 100 mg of distal colon tissue per group using the TRIzol method. RNA concentration and purity were determined on a NanoDrop spectrophotometer, followed by reverse transcription to generate cDNA. Real-time quantitative polymerase chain reaction (qPCR) was performed using SYBR Green chemistry in a 20 µL reaction system comprising 2 µL of cDNA template, 0.4 µM each of forward and reverse primers, and 10 µL of SYBR Master Mix (Beyotime, Batch No: D7601S, China). The thermal cycling protocol consisted of an initial denaturation at 95 °C for 30 s, followed by 40 cycles of 95 °C for 5 s, 60 °C for 30 s, and 72 °C for 30 s. Primer specificity was confirmed by melting curve analysis. Glyceraldehyde-3-phosphate dehydrogenase (GAPDH) served as the endogenous reference gene, and relative expression levels of TNF-α, IL6, Nfkb, inhibitor of nuclear factor kappa B kinase subunit beta (Ikbkb), and Rage mRNA were calculated using the $2^{-\Delta\Delta Ct}$ method (Table 1).

2.8 Western Blot

Approximately 100 mg of distal colon tissue from each group was collected and homogenized in radioimmunoprecipitation assay (RIPA) lysis buffer (Beyotime, Batch No: P0013B, China). Following homogenization, lysates were centrifuged at 12,000 rpm for 15 min at 4 °C. The supernatant was collected, and protein concentration was determined by the bicinchoninic acid (BCA) assay (Beyotime, Batch No: P0009, China). Thirty-five micrograms of protein per sample were resolved by sodium dodecyl sulfate-polyacrylamide gel electrophoresis (SDS-PAGE) (Beyotime, Batch No: P0014D, China) and electrotransferred onto polyvinylidene fluoride (PVDF) membranes. Membranes were blocked with 5% non-fat milk for 1 h at room temperature, then incubated overnight at 4 °C with the following primary antibodies: Anti-RAGE (Abcam, Batch No: ab172473, UK, 1:1000), Anti-inhibitor of nuclear factor kappa-B kinase (IKK) beta (Abcam, Batch No: ab32135, UK, 1:1000), Anti-inhibitor of kappa B (IKB) alpha (Abcam, Batch No: ab7217, UK, 1:2000), Anti-NF-κB p65 (Abcam, Batch No: ab16502, UK, 1:2000), Anti-NF-κB p65 (Abcam, Batch No: ab76302, UK, 1:500), Anti-p53 (Abcam, Batch No: ab211020, UK, 1:1000), Anti-Bcl-2-associated X protein (Bax) (Abcam, Batch No: ab32503, UK, 1:1000), Anti-B-cell lymphoma 2 (Bcl-2) (Abcam, Batch No: ab16904, UK, 1:1000), and Anti-Cleaved Caspase-3 (Abcam, Batch No: ab214430, UK, 1:500). The following day, membranes were washed with Tris-buffered saline containing Tween 20 (TBST) (Beyotime, Batch No: ST671, China) and incubated with horseradish peroxidase (HRP)-conjugated goat anti-rabbit or anti-mouse immunoglobulin G (IgG) secondary antibodies (Abcam, Batch No: ab97051, UK, 1:5000) for 1 h at room temperature. Protein bands were visualized using an enhanced chemiluminescence (ECL) substrate (Beyotime, Batch No: P0018S, China) and captured with a gel documentation system. GAPDH (Abcam, Batch No: ab181602, UK, 1:5000) was used as the loading control, and relative protein expression was quantified using ImageJ.

2.9 Statistical Analysis

All statistical analyses were conducted using standard software packages. Data are expressed as mean ± standard deviation (SD). Normality of data distribution was assessed using the Shapiro-Wilk test, and homogeneity of variance was evaluated using Levene's test prior to performing analysis of variance (ANOVA). Multiple group comparisons were performed using one-way ANOVA followed by Tukey's honestly significant difference (HSD) post hoc test. Statistical significance was defined as a two-tailed $p < 0.05$. Experiments utilized a sample size of n = 5 per group for histological, molecular, and serological analyses, determined based on preliminary data and power analysis. For multi-endpoint comparisons, Bonferroni correction was applied to control the family-wise error rate. Statistical

Table 1. Primers sequence.

Gene	Forward primer (5′–3′)	Reverse primer (5′–3′)	Product size (bp)
Rage	CCTGTAGCCCACGTCGTAG	GGGAGTAGACAAGGTACAACCC	166
Ikbkb	TAGTCCTTCCTACCCCAATTTCC	TTGGTCCTTAGCCACTCCTTC	160
Nfkb	CGAGCCAGAGTCATTAGCCA	CGTAGTAGTCCGTGTCTGCC	183
Il6	CCGTCTGTGCTGCTTCGTA	GGTGTAGCCCTCTTCGTCAG	177
Tnf	CCTTCTACGACGATGCCCTC	GTTGCTGAGGTTGGCGTAGA	168
Gapdh	GGCTGTATTCCCCTCCATCG	CCAGTTGGTAACAATGCCATGT	127

Rage, receptor for advanced glycation end products; Ikbkb, inhibitor of nuclear factor kappa B kinase subunit beta; Nfkb, nuclear factor kappa B; Il6, interleukin 6; Tnf, tumor necrosis factor; Gapdh, glyceraldehyde-3-phosphate dehydrogenase.

Package for the Social Sciences (SPSS) 22.0 (IBM, USA) was used for all analyses, and graphical outputs were generated using GraphPad Prism 9.0.

3. Results

3.1 Identification of the PRA Fingerprint

The paeoniflorin reference standard and PRA samples were analyzed by UPLC at 230 nm. The standard paeoniflorin exhibited retention times of 16.360, 16.302, and 16.295 min across three replicate injections (mean: 16.319 min; relative standard deviation (RSD) = 0.20%), with peak areas of 94.003, 98.642, and 98.929, confirming adequate instrument precision (Fig. 1A). In the PRA sample, the corresponding peaks appeared at 16.287, 16.285, and 16.277 min (mean: 16.283 min), with a deviation of less than 0.05 min from the standard. Peak areas were 18.107, 18.118, and 18.305 mAU·min (RSD = 0.59%) (Fig. 1B). Additional common peaks were also detected, reflecting the multi-component nature of PRA. These findings confirmed the presence of paeoniflorin in the PRA sample with satisfactory reproducibility across three injections, meeting fingerprint analysis requirements. Similarity indices among the three replicate chromatograms all exceeded 0.99, and RSDs of major peak areas were below 1.0%, demonstrating good analytical reproducibility. The fingerprint profile captured multiple common peaks beyond paeoniflorin, reflecting the multi-component chemical spectrum of PRA.

3.2 Effects of PRA on Intestinal Morphology and Function in IBS-D Model Mice

Compared with blank animals, model mice showed a deteriorated general condition, including lethargy, reduced locomotor activity, dull fur, diminished food consumption, and blunted weight gain. Stools were loose and unformed, with significantly increased fecal water content, accelerated small intestinal transit, and shortened small intestinal length ($p < 0.01$), collectively confirming successful IBS-D model establishment (Fig. 2A). Histological examination revealed disorganized mucosal architecture, irregular villous morphology, mild epithelial injury, inflammatory cell infiltration, and interstitial edema ($p < 0.01$) (Fig. 2B). The NF-κB-positive area in distal colon tissue was significantly enlarged ($p < 0.01$) (Fig. 2C), and expression of the tight junction proteins ZO-1, Occludin, and Claudin-1, together with the mucus barrier protein MUC2, was substantially diminished, indicating compromised intestinal barrier function ($p < 0.01$) (Fig. 2D). Serum concentrations of IL-6, TNF-α, NF-κB, IL-1β, and MCP-1 were markedly elevated in model mice ($p < 0.01$) (Fig. 2E), indicative of a pronounced low-grade inflammatory state and activation of inflammatory signaling. PRA treatment dose-dependently improved the general condition of mice. Body weight and food intake gradually recovered, stool consistency improved, fecal water content decreased, and small intestinal transit rate was reduced. PRA effectively lowered serum levels of IL-6, TNF-α, NF-κB, IL-1β, and MCP-1 ($p < 0.05$). Concurrently, PRA restored the structural integrity of the intestinal mucosa, reduced inflammatory cell infiltration, and reversed the increase in colonic NF-κB-positive expression ($p < 0.05$). Moreover, expression of ZO-1, Occludin, Claudin-1, and MUC2 was restored to varying degrees.

Following PRA administration, dose-dependent improvements were noted across multiple parameters: body weight and food consumption progressively normalized, stool form improved with reduced fecal hydration, and small intestinal transit velocity decreased. Serum concentrations of IL-6, TNF-α, NF-κB, IL-1β, and MCP-1 were significantly reduced by PRA ($p < 0.05$). Histologically, PRA reinstated mucosal architectural integrity, curtailed inflammatory cell infiltration, and diminished NF-κB immunoreactivity ($p < 0.05$). Additionally, the expression levels of ZO-1, Occludin, Claudin-1, and MUC2 were partially to fully restored across PRA treatment groups (Fig. 2).

3.3 Analysis of Potential Targets and Pathways of PRA Intervention in IBS-D Model Mice

To characterize the molecular basis of PRA's therapeutic action on IBS, distal colon tissue transcriptomic profiling was combined with network pharmacology-based prediction of PRA bioactive constituents. At the transcriptomic level, 477 DEGs were identified between the blank and model groups (220 downregulated, 257 upregulated), while 114 DEGs were detected between the model and PRA groups (43 downregulated, 71 upregulated), with

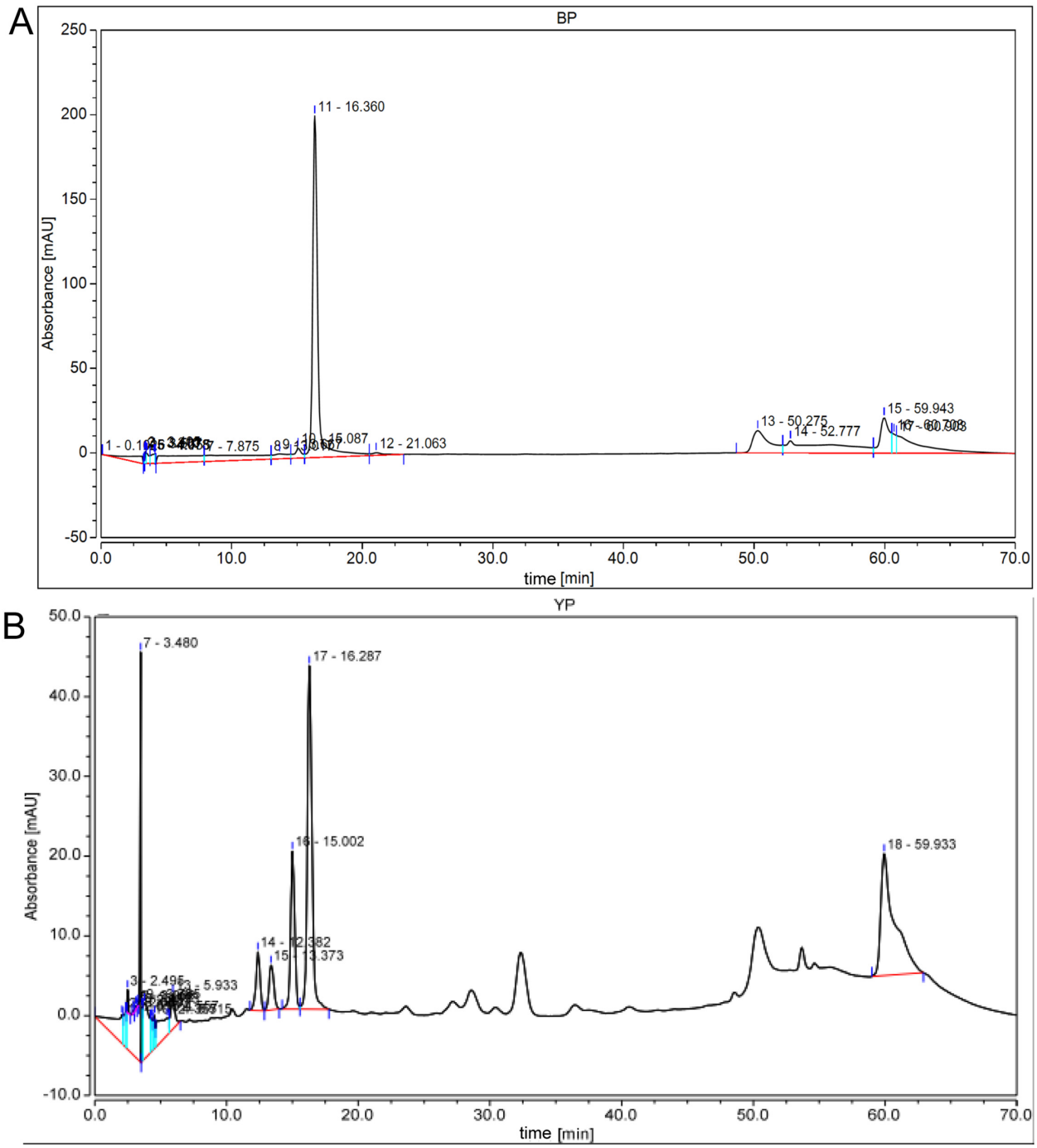


Fig. 1. Construction of the fingerprint pattern of PRA. (A) Three replicate chromatograms of the paeoniflorin reference substance, showing the peak at approximately 16.3 min corresponding to paeoniflorin. (B) Three replicate chromatograms of the PRA sample, with the peak at approximately 16.3 min corresponding to paeoniflorin and additional common peaks reflecting the multi-component characteristics of PRA. All chromatograms were detected at 230 nm using a C18 column with gradient elution. The peak at approximately 16.3 min was identified as paeoniflorin based on retention time alignment with the authentic reference standard (deviation <0.05 min). Similarity indices among replicate chromatograms exceeded 0.99, confirming analytical reproducibility. The chromatograms shown are UV chromatograms detected at 230 nm, not extracted-ion chromatograms from mass spectrometry. PRA, Paeoniae Radix Alba.

63 genes modulated by PRA intervention (Fig. 3A–D). WGCNA identified four co-expression modules, of which the turquoise module showed the strongest correlation and contained the largest gene set (40 genes) (Fig. 3E–H). These 40 genes were submitted to the STRING database for PPI network construction, yielding the top 10 hub genes by in-degree ranking: nuclear factor kappa B subunit 1 (NFKB1), matrix metalloproteinase-9 (MMP9), TNF, IL6,

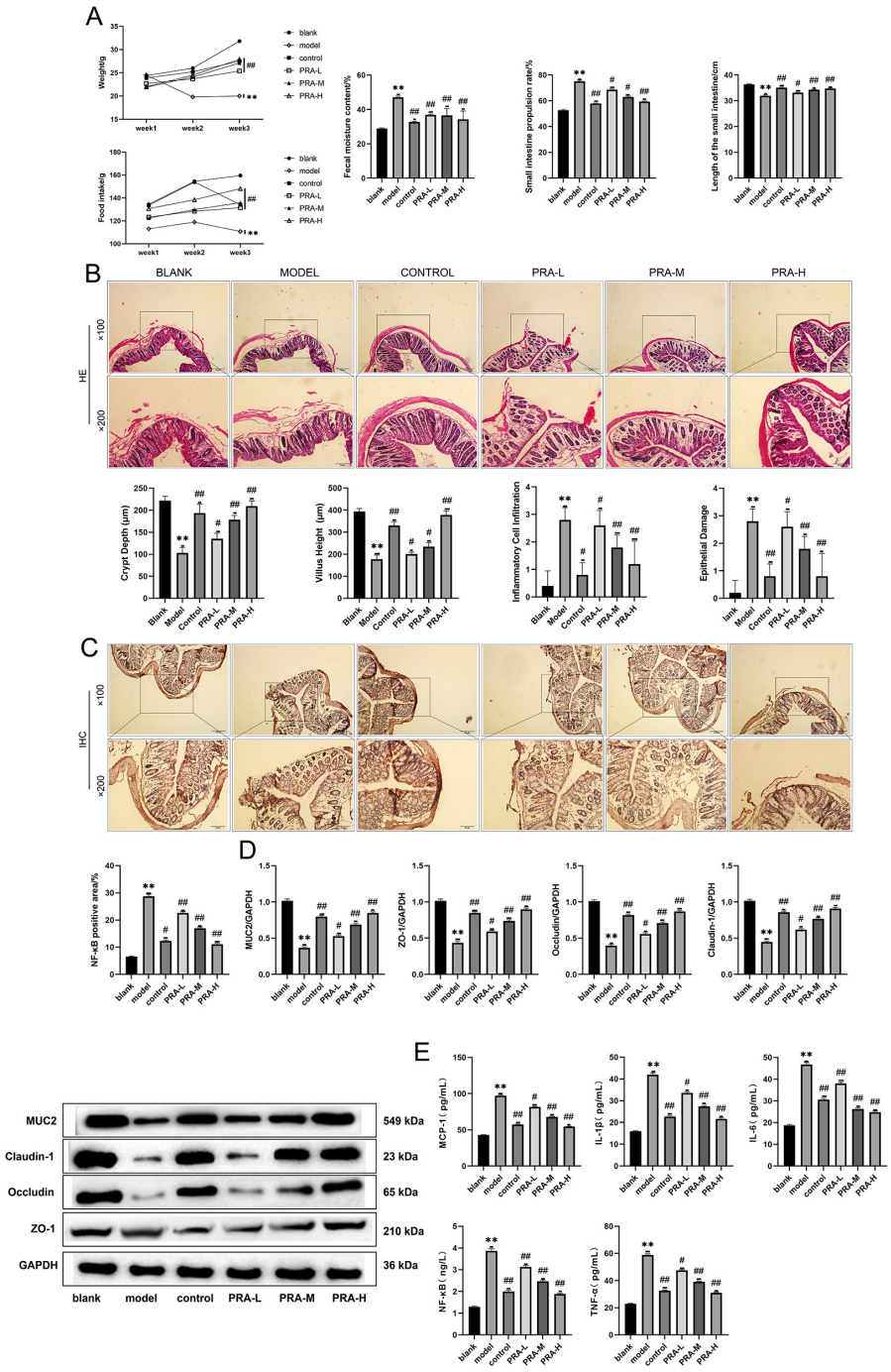


Fig. 2. Effects of PRA on intestinal morphology and function in each group of mice. (A) General status of mice in each group, including body weight, food intake, fecal water content, small intestinal transit rate, and small intestinal length, n = 5; compared with the blank group, $^{**}p < 0.01$; compared with the model group, $^{\#\#}p < 0.01$, $^{\#}p < 0.05$. (B) HE staining of distal colon tissue of mice in each group, Scale bar: 100 μm (×100), Scale bar: 50 μm (×200), n = 5; compared with the blank group, $^{**}p < 0.01$, compared with the model group, $^{\#}p < 0.05$, $^{\#\#}p < 0.01$. (C) IHC staining of distal colon tissue of mice in each group, Scale bar: 100 μm (×100), Scale bar: 50 μm (×200), n = 5; compared with the blank group, $^{**}p < 0.01$; compared with the model group, $^{\#\#}p < 0.01$, $^{\#}p < 0.05$. (D) Western blot analysis of ZO-1, Occludin, Claudin-1, and MUC2 protein expression in distal colon tissue, normalized to GAPDH as an internal loading control, n = 5; compared with the blank group, $^{**}p < 0.01$; compared with the model group, $^{\#\#}p < 0.01$, $^{\#}p < 0.05$. (E) Expression of inflammatory cytokines in the serum of mice in each group, n = 5, compared with the blank group, $^{**}p < 0.01$; compared with the model group, $^{\#\#}p < 0.01$, $^{\#}p < 0.05$. Statistical comparisons were performed using one-way ANOVA followed by Tukey's HSD post hoc test. HE, hematoxylin-eosin; IHC, immunohistochemistry; ZO-1, zonula occludens-1; MUC2, mucin 2; ANOVA, analysis of variance; HSD, honestly significant difference.

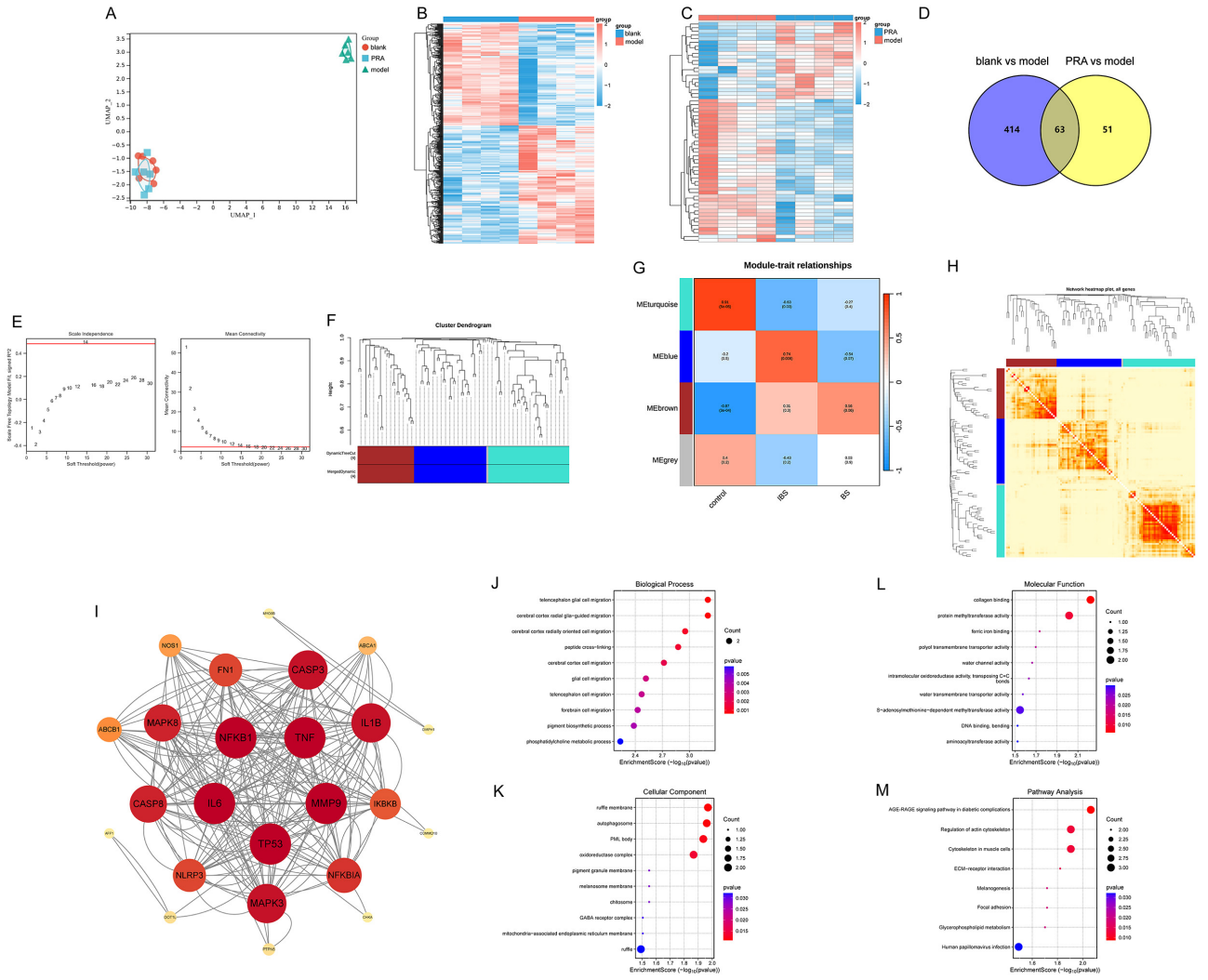


Fig. 3. Transcriptomics results of PRA in the treatment of IBS-D. (A) Uniform manifold approximation and projection (UMAP) analysis of transcriptomics data, n = 6. (B,C) DEG analysis among the control, IBS, and PRA groups. (D) Venn diagram showing 63 DEGs regulated by PRA. (E) Parameter selection for WGCNA network construction (power value = 14). (F) Gene clustering dendrogram based on the dissTOM matrix from WGCNA analysis. (G) Trait-module association heatmap from WGCNA analysis. (H) Heatmap of all genes from WGCNA analysis. (I) PPI network analysis of 40 genes. (J–L) GO analysis: BP, CC, and MF. (M) KEGG pathway analysis. BS, Baishao; IBS, irritable bowel syndrome; IBS-D, diarrhea-predominant irritable bowel syndrome; DEG, differentially expressed gene; WGCNA, weighted gene co-expression network analysis; dissTOM, dissimilarity topological overlap matrix; PPI, protein-protein interaction; GO, Gene Ontology; BP, biological process; CC, cellular component; MF, molecular function; KEGG, Kyoto Encyclopedia of Genes and Genomes.

TP53, interleukin 1 beta (IL1B), mitogen-activated protein kinase 3 (MAPK3), CASP3, MAPK8, and CASP8 (Fig. 3I). GO enrichment analysis produced 138 terms: 106 BP terms (including cerebral cortex radial glia-guided migration, telencephalon glial cell migration, and cerebral cortex radially oriented cell migration); 14 CC terms (including ruffle membrane, autophagosome, and promyelocytic leukemia [PML] body); and 18 molecular function (MF) terms (including collagen binding, protein methyltransferase activity, and ferric iron binding) (Fig. 3J–L). KEGG pathway analysis showed enrichment predominantly in the NF-κB, cytoskeleton in muscle cells, and advanced glycation end product (AGE)-RAGE signaling pathways ($p < 0.05$) (Fig. 3M). In parallel, network pharmacology screening of the TCMSP database identified 13 active PRA compounds with 236 corresponding targets. Cross-referencing with 263 IBS-related targets retrieved from GeneCards, SymMap and OMIM yielded 36 overlapping targets (Fig. 4A). Drug-component-target network analysis highlighted kaempferol, benzoyl paeoniflorin, lactiflorin, paeoniflorin, and albiflorin as the core compounds (Fig. 4B). PPI network analysis of the overlapping targets identified the top 10 core targets (TNF, IL6, AKT1, B-cell lymphoma 2 [BCL2], signal transducer and acti-

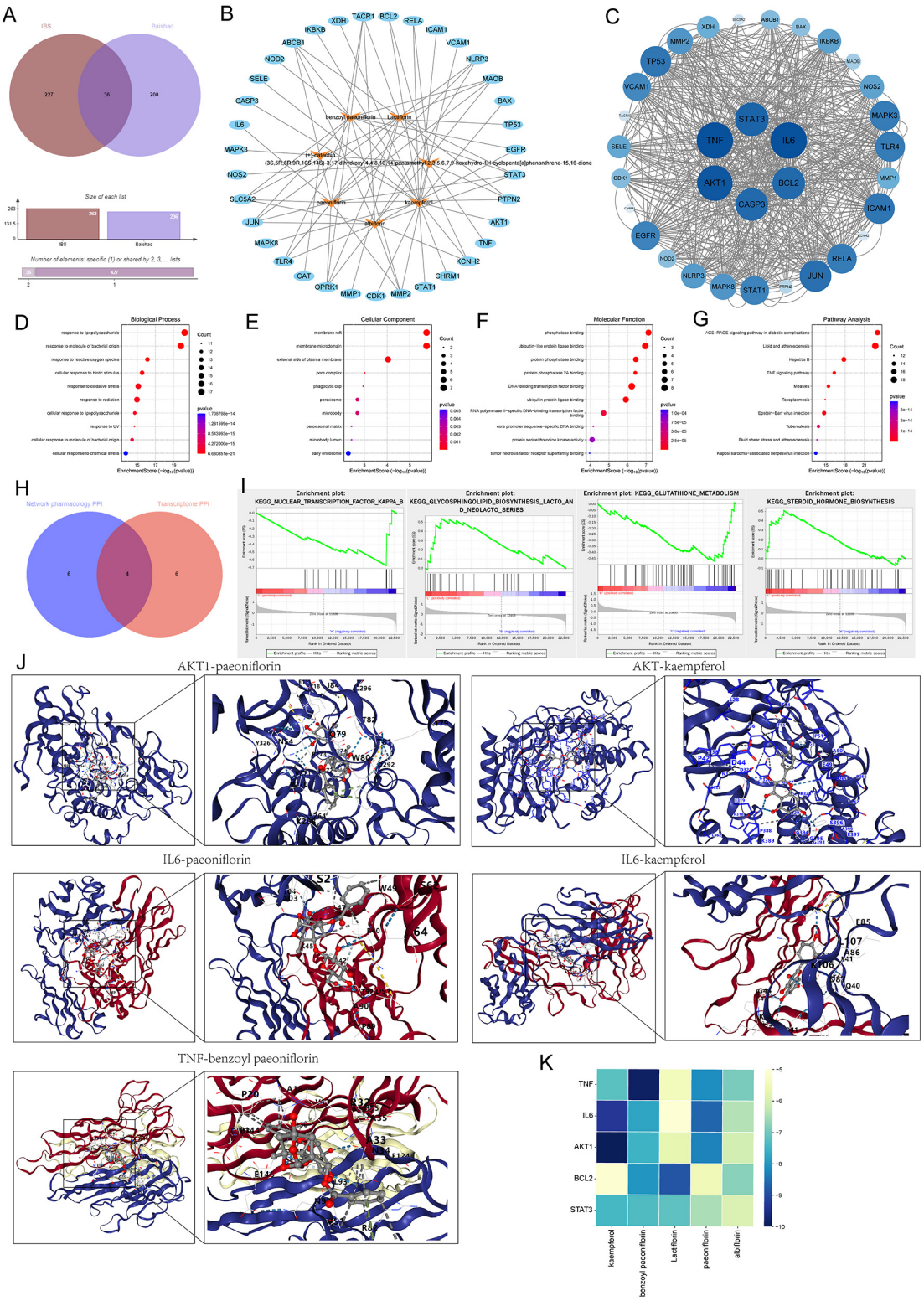


Fig. 4. Network pharmacology results of PRA in the treatment of IBS. (A) Venn diagram of potential targets of PRA in the treatment of IBS-D. (B) "Drug-component-target" network of PRA in the treatment of IBS-D. (C) PPI network analysis of 36 targets of PRA in regulating IBS-D. (D–F) GO analysis: BP, CC, and MF. (G) KEGG pathway analysis. (H) Venn diagram showing the overlapping core targets between transcriptomics and network pharmacology. (I) GSEA of the overlapping targets, including NF-κB, glutathione metabolism, glycosphingolipid biosynthesis – lacto and neolacto series, and steroid hormone biosynthesis. (J) Molecular docking diagrams of AKT1-paeoniflorin, AKT-kaempferol, IL6-paeoniflorin, IL6-kaempferol, and TNF-benzoyl paeoniflorin. (K) Heatmap of molecular docking binding energies. GSEA, gene set enrichment analysis; AKT1, AKT serine/threonine kinase 1.

vator of transcription 3 [STAT3], CASP3, TP53, ICAM1, MAPK3 and Jun proto-oncogene[JUN]) by degree values (Fig. 4C). GO and KEGG enrichment analyses indicated that these targets were primarily involved in responses to lipopolysaccharide and reactive oxygen species, associated with membrane rafts, membrane microdomains, and the external plasma membrane, and exerted functions including phosphatase binding, ubiquitin-like protein ligase binding, and protein phosphatase binding. Pathway enrichment showed concentration in the AGE/RAGE and NF-κB signaling pathways (Fig. 4D–G). Through the PPI analysis in network pharmacology and transcriptomics, we identified four intersecting targets, namely IKBKB, IL6, TNF, and TP53 (Fig. 4H). Gene set enrichment analysis (GSEA) further confirmed that IKBKB, IL6, TNF, and TP53 were core targets of PRA in IBS-D treatment, enriched in the NF-κB pathway (Fig. 4I). Molecular docking of the top five compounds and targets showed that all binding energies were below –5 kcal·mol^{-1} (Fig. 4J,K). The network pharmacology findings thus corroborated the transcriptomic results, demonstrating strong concordance in identifying the AGE/RAGE and NF-κB pathways as central to PRA's therapeutic mechanism.

Importantly, the key targets predicted by network pharmacology exhibited a high degree of concordance with the differentially expressed genes identified through transcriptomic analysis, reinforcing the robustness of these findings and suggesting mechanistic consistency in the pharmacological actions of PRA.

3.4 PRA Ameliorated Inflammation in IBS Mice by Regulating the RAGE/NF-κB Pathway

To elucidate the mechanism underlying PRA's attenuation of the inflammatory response in IBS, the expression profiles of RAGE/NF-κB pathway-associated proteins and inflammatory cytokines were assessed. Relative to the blank group, serum levels of IL-6, TNF-α, IL-1β, and EDN1 in the model group were markedly elevated ($p < 0.01$), confirming successful induction of a robust inflammatory response in the IBS model (Fig. 5A). Protein expression of RAGE, IKBKB, IκBα, and p-p65/p65 was also significantly increased in the model group ($p < 0.01$), indicating marked activation of the RAGE/NF-κB signaling cascade (Fig. 5B). Concurrently, mRNA expression of Rage, Ikbkb, Nfkb, Il6, and Tnf was significantly upregulated in the model group ($p < 0.01$) (Fig. 5C). Immunofluorescence analysis further revealed strongly enhanced positive staining for RAGE and NF-κB in the distal colon tissue of model group mice (Fig. 5D). HE staining showed that the mucosa and surface of the distal colon tissue in the model group mice were incomplete and were accompanied by inflammatory infiltration (Fig. 5E). Compared with the model group, both the PRA-H and FPS-ZM1 groups exhibited significant reductions in IL-6, TNF-α, IL-1β, and EDN1 levels ($p < 0.01$) and downregulation of Rage, Ikbkb, Nfkb, Il6, and Tnf mRNA expression ($p < 0.01$). Protein expression of RAGE, IKBKB, IκBα, and p-p65/p65 was also significantly diminished in the PRA-H and FPS-ZM1 groups relative to the IBS group ($p < 0.01$), positive staining for RAGE and NF-κB was attenuated. Of note, all parameters in the PRA-H + FPS-ZM1 group showed further improvement compared with either the PRA-H or FPS-ZM1 group alone, although there was no statistical significance between them, suggesting that PRA and the RAGE inhibitor may synergistically inhibit the activation of the RAGE/NF-κB pathway. Collectively, these results indicated that PRA significantly inhibited activation of the RAGE/NF-κB signaling pathway in the distal colon tissue of IBS mice and diminished the release of inflammatory cytokines, thereby ameliorating the IBS-associated inflammatory state.

3.5 PRA Inhibited Apoptosis in Distal Colon Tissue of IBS Mice by Regulating the RAGE/NF-κB Pathway

The candidate targets of PRA for IBS treatment identified through network pharmacology encompassed not only inflammatory mediators but also the apoptosis-related factor TP53. To further characterize the protective effects of PRA on distal colon tissue injury in IBS mice, the extent of apoptosis in distal colon tissue across all groups was evaluated. Relative to the blank group, protein expression of TP53, Bax, and cleaved-caspase-3 in the distal colon tissue of the model group was significantly elevated, whereas Bcl-2 protein expression was significantly reduced ($p < 0.01$) (Fig. 6A). Furthermore, the number of TUNEL-positive cells and the apoptotic index in distal colon tissue were significantly higher than those in the control group ($p < 0.01$), indicating that the IBS model induced substantial apoptosis in distal colon tissue (Fig. 6B). Immunohistochemical analysis revealed a significantly increased TP53-positive area in the distal colon tissue of the model group ($p < 0.01$) (Fig. 6C). Compared with the model group, both the PRA-H and FPS-ZM1 groups significantly reduced protein expression of TP53, Bax, and cleaved-caspase-3 while upregulating Bcl-2 expression ($p < 0.01$). Concurrently, the TP53-positive area was diminished on immunohistochemistry, and both TUNEL-positive cell counts and the apoptotic index were significantly reduced ($p < 0.01$). Notably, the improvement in apoptotic parameters in the PRA-H + FPS-ZM1 group was more pronounced than in either the PRA-H or FPS-ZM1 group alone, although there was no statistical significance between them, indicating that the combination of PRA and the RAGE inhibitor further alleviated distal colon tissue apoptosis in IBS mice.

4. Discussion

As the most prevalent functional gastrointestinal condition, IBS is currently classified within the disorders of gut-brain interaction (DGBI) spectrum and is clinically defined by recurrent abdominal pain, bloating, and disturbed bowel habits [25,26]. IBS-D represents the largest clin-

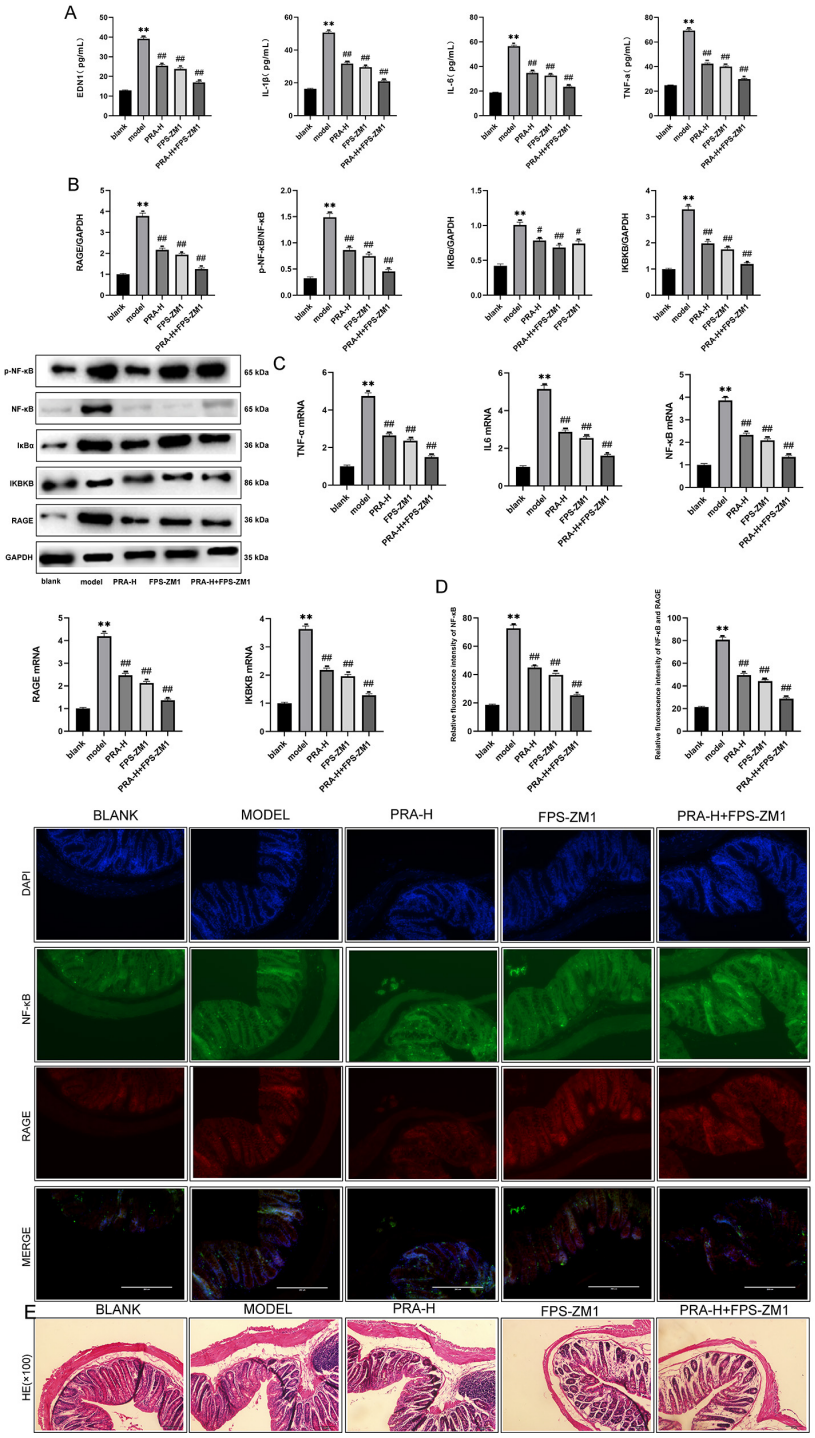


Fig. 5. Regulatory effect of PRA on the AGE/RAGE/NF-κB pathway in the IBS mouse model. (A) Serum levels of inflammatory cytokines (EDN1, IL-6, TNF-α, and IL-1β) in each group (n = 5). (B) Representative Western blot bands and quantitative analysis of RAGE, IKBKB, NF-κB, p-NF-κB, and IκBα protein expression in distal colon tissues. GAPDH was used as the loading control. Lanes from left to right represent the blank, model, PRA-H, FPS-ZM1, and PRA-H+FPS-ZM1 groups, respectively. (C) Relative mRNA expression levels of Rage, Ikbkb, Nfkb, Il6, and Tnf determined by qPCR (n = 5). (D) Representative immunofluorescence images showing the colocalization and expression of RAGE (red) and NF-κB (green) in distal colon sections; cell nuclei were counterstained with DAPI (blue), Scale bar: 200 μm, the bar charts represent the relative fluorescence intensity of RAGE and NF-κB (n = 5). (E) Representative hematoxylin and eosin (H&E) staining of distal colon tissue sections to assess histopathological changes, Scale bar: 50 μm, All data are presented as the mean ± SD (n = 5). $^{**}p < 0.01$ vs. blank group; $^{\#\#}p < 0.01$ and $^{\#}p < 0.05$ vs. model group. AGE, advanced glycation end product; PRA-L, low-dose PRA; PRA-M, medium-dose PRA; PRA-H, high-dose PRA; qPCR, real-time quantitative polymerase chain reaction; DAPI, 4′,6-diamidino-2-phenylindole; SD, standard deviation.

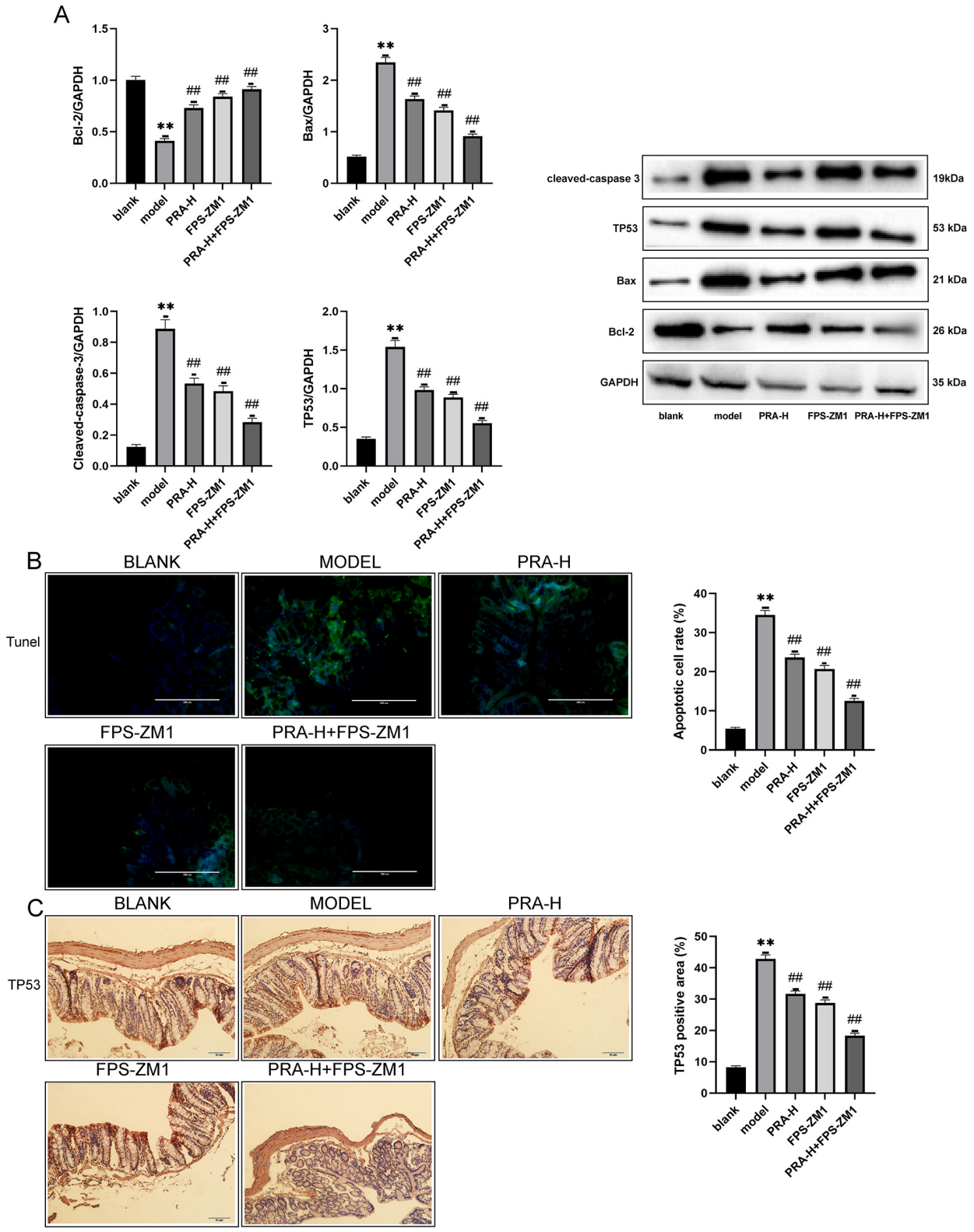


Fig. 6. Regulatory effect of PRA on apoptosis levels in the IBS mouse model. (A) Protein expression of TP53, Bax, cleaved-caspase-3, and Bcl-2 in the distal colon tissue of mice in each group, n = 5, compared with the blank group, $^{**}p < 0.01$; compared with the model group, $^{\#\#}p < 0.01$. (B) Apoptosis rate in the distal colon tissue of mice in each group, Scale bar: 200 μm, n = 5, compared with the blank group, $^{**}p < 0.01$; compared with the model group, $^{\#\#}p < 0.01$. (C) TP53 expression in the distal colon tissue of mice in each group, Scale bar: 50 μm, n = 5, compared with the blank group, $^{**}p < 0.01$; compared with the model group, $^{\#\#}p < 0.01$. TP53, tumor protein p53; Bax, Bcl-2-associated X protein; Bcl-2, B-cell lymphoma 2.

ical subgroup and is typically accompanied by fecal urgency, loose or watery stools, heightened visceral pain sensitivity, and reduced quality of life, frequently co-occurring with anxiety, depression, and sleep disturbances that collectively impose a substantial medical and societal burden [27]. Over the past decade, the conceptual framework surrounding IBS-D has evolved from a purely functional label to a multifactorial disorder involving low-grade mucosal inflammation, compromised epithelial barrier integrity, gut microbiota dysbiosis, and neuroendocrine dysregulation. Available therapeutic options, including antispasmodics, antidiarrheals, 5-hydroxytryptamine (5-HT) modulators, and psychological therapies—are limited by marked interindividual variability in response, high relapse rates upon discontinuation, and inadequate long-term safety data [28]. PRA is a widely used botanical remedy whose anti-inflammatory, antioxidant, immunomodulatory, smooth muscle relaxant, and mucosal barrier-protective properties have been substantiated by modern pharmacological research. The RAGE and its downstream inflammatory cascades occupy a central position in chronic intestinal inflammation and barrier damage, with aberrant RAGE activation having been documented across multiple intestinal pathologies [29,30]. Elucidating the mechanism by which PRA modulates IBS-D through the RAGE pathway thus carries both scientific novelty and translational significance.

From a wider pathophysiological vantage point, IBS-D is increasingly recognized as a multifaceted disorder encompassing low-grade intestinal inflammation, epithelial barrier dysfunction, altered gastrointestinal motility, immune activation, and stress-related gut disturbances. The present findings situate PRA within this integrated pathogenic framework: by simultaneously modulating inflammatory cytokine release, tight junction protein expression, mucus secretion, and epithelial apoptosis, PRA appears to function as a multi-target regulator rather than a conventional anti-inflammatory agent. The AGE/RAGE/NF-κB signaling cascade may serve as a mechanistic nexus interconnecting these seemingly disparate pathological processes. When RAGE is engaged by AGEs and other ligands, it can trigger NF-κB-driven transcription of pro-inflammatory cytokines, which in turn disrupt tight junctions, deplete mucus, sensitize pain pathways, and promote epithelial cell death. The observation that PRA attenuated this cascade at multiple levels from upstream RAGE expression through downstream cytokine release, barrier protein restoration, and apoptosis inhibition—supports the interpretation that its therapeutic effects stem from coordinated multi-pathway modulation rather than suppression of a single target. This multi-target characteristic is especially pertinent for a complex disorder such as IBS-D, where no single mechanism fully accounts for the disease phenotype.

An integrated analytical framework merging network pharmacology with transcriptomic profiling was deployed to unravel the molecular basis of PRA's therapeutic efficacy against IBS-D. Profiling of intestinal transcriptomes revealed widespread transcriptional alterations between healthy and diseased animals. Through WGCNA, gene modules displaying significant disease-phenotype correlations were delineated, with hub genes NFKB1, TNF, IL6, IL1B, CASP3, and TP53 clustering predominantly within inflammatory amplification, immune activation, and programmed cell death regulatory networks. This gene signature indicates that the IBS-D phenotype is intrinsically linked to concurrent inflammatory responses and mucosal tissue injury. Complementary network pharmacology screening designated paeoniflorin and benzoyl paeoniflorin as the leading bioactive constituents driving PRA's anti-IBS-D activity. PPI network topology analysis of overlapping targets further highlighted TNF, IL6, AKT1, BCL2, STAT3, CASP3, TP53, and JUN as the most interconnected nodes. A striking concordance was observed between the transcriptome-derived DEGs and the network pharmacology-predicted targets, underscoring the internal consistency of PRA's pharmacological action spectrum. Notably, pathway enrichment analyses from both analytical approaches converged on the AGE/RAGE cascade as a top-ranked candidate mechanism. Historically, the AGE-RAGE axis has been extensively characterized as a pathological driver in diabetic complications, cardiovascular pathology, and renal disease, where its engagement precipitates NF-κB nuclear translocation via JAK, PI3K, and MAPK cascades, culminating in transcriptional upregulation of IL-6, TNF-α, and allied pro-inflammatory mediators [31]. More recently, a growing body of evidence has implicated RAGE signaling in the maintenance of intestinal epithelial integrity, regulation of mucosal permeability, and amplification of local inflammatory responses [32,33]. Multiple natural products and traditional herbal formulations have been shown to counteract IBS-D or colitis through dampening of NF-κB, MAPK, and NLRP3 inflammasome pathways [34,35,36,37]. Specifically, Shengjiang San was demonstrated to attenuate sepsis-provoked intestinal injury by harnessing Lactobacillus-derived metabolites to reprogram macrophage polarization via NF-κB and TGF-β signaling routes [38]. The AGE/RAGE/NLRP3 axis has further been implicated as a critical mediator in colitis, with evidence that traditional Chinese medicine interventions can reverse its activation [39]. Additionally, NEDD4 binding protein 3 (N4BP3) has recently been shown to facilitate K48-linked IκBα ubiquitination, thereby triggering TLR4/NF-κB signaling in inflammatory bowel disease—further emphasizing the centrality of NF-κB to intestinal inflammatory pathology [40]. Complementarily, meta-analytic evidence supports that mesalazine combined with traditional Chinese medicines yields superior efficacy and safety profiles in mild-to-moderate ulcerative colitis, rein-

forcing the value of integrative therapeutic strategies for intestinal inflammatory conditions [41].

Prior work has established that chemical irritants alone, while capable of eliciting diarrhea and mucosal damage, inadequately recapitulate the psychophysiological stress dimensions inherent to IBS-D. Conversely, stress-exclusive paradigms, though better approximating gut-brain axis perturbations, frequently fail to reliably induce overt diarrheal symptoms and barrier compromise [42]. The current study therefore adopted a hybrid modeling strategy coupling acetic acid colonic instillation with restraint and tail-compression stress. This dual-insult design was intended to more faithfully reproduce the composite pathogenic features of IBS-D, simultaneously capturing both local intestinal hypersensitivity and central stress axis engagement. Phenotypically, model group mice exhibited depressed behavioral status, poor coat condition, decreased spontaneous activity, reduced caloric intake, blunted or negative weight trajectories, elevated fecal hydration, and accelerated small bowel transit, collectively signifying effective IBS-D-like symptom induction. PRA administration reversed these abnormalities: general behavioral status improved, body weight accrual normalized, diarrheal features subsided, and small intestinal transit velocity decelerated, pointing to a meaningful regulatory influence of PRA on both systemic symptom profiles and gut motility dysregulation in IBS-D.

In the model group, intestinal expression of the tight junction proteins ZO-1, Occludin, and Claudin-1, along with the secretory mucin MUC2, was markedly diminished—pointing to concurrent disruption of both mechanical and mucus layers of the intestinal barrier. When paracellular permeability is increased, luminal antigens and microbial products gain access to the underlying mucosal immune compartment, perpetuating a self-sustaining cycle of low-grade inflammation and visceral afferent sensitization [43]. PRA treatment significantly reinstated expression of these junctional and mucin proteins, indicative of a direct barrier-protective action. The model group also displayed substantially elevated serum and colonic concentrations of IL-6, TNF-α, IL-1β, MCP-1, and EDN1, reflecting an activated low-grade inflammatory state—a finding that aligns with the contemporary understanding that IBS-D, while lacking the overt tissue destruction of inflammatory bowel disease, is nonetheless accompanied by mild mucosal inflammatory infiltrate and dysregulated cytokine production. PRA intervention substantially decreased these inflammatory mediators, demonstrating pronounced anti-inflammatory activity. This anti-cytokine effect is consistent with a broader literature documenting that suppression of IL-6, TNF-α, and IL-1β release and consequent attenuation of mucosal low-grade inflammation—constitutes a shared mechanism through which diverse natural products and botanical formulations ameliorate IBS-D symptoms [44,45,46,47]. Moreover, natural polysaccharides have been shown to counteract intestinal barrier damage via gut microbiota reshaping, lending further support to the barrier-protective capacity of botanical agents [48]. Indeed, emerging evidence demonstrates that natural products can restructure the intestinal microbial ecosystem and mitigate ulcerative colitis through modulation of microbiota composition and metabolic output, highlighting the therapeutic promise of microbiota-directed natural product interventions in intestinal disorders [49].

These observations prompt a critical mechanistic question: does the barrier-restoring action of PRA represent a primary pharmacological effect, or is it an indirect consequence of AGE/RAGE/NF-κB axis suppression? The current data favor a bidirectional interplay over a strictly linear causality. On one side, NF-κB activation is known to directly transcriptionally repress tight junction protein genes and loosen epithelial permeability, implying that PRA's anti-inflammatory properties may secondarily promote barrier recovery. On the other side, the swift restitution of ZO-1, Occludin, and Claudin-1 expression observed following PRA treatment hints at a direct junction-protective mechanism that operates independently of cytokine suppression. The reciprocal and self-reinforcing nature of these processes—where inflammatory mediators drive junctional dissolution, mucus layer depletion, and epithelial cell death in a cascading sequence—highlights why multi-target botanical agents such as PRA may hold therapeutic advantages over single-mechanism pharmacological interventions.

Advanced glycation end products and their cognate receptor RAGE have garnered increasing recognition as pivotal amplifiers of intestinal inflammation and barrier compromise. Endogenous RAGE ligands, including S100 calgranulins and high mobility group box 1 (HMGB1), have been demonstrated to disrupt intestinal epithelial tight junctions, activate NF-κB-driven transcription, and promote neutrophil chemotaxis, pro-inflammatory cytokine secretion, and mucosal tissue injury [50,51,52,53]. Clinical and experimental studies have documented upregulated RAGE expression in both inflammatory bowel disease patients and experimental colitis models, where pharmacological blockade of RAGE signaling produced significant attenuation of disease severity [54,55]. These prior findings resonate with the present results, suggesting that dysregulated RAGE pathway activation is not restricted to organic intestinal inflammatory diseases but likely also contributes to the pathobiology of functional bowel disorders such as IBS-D, which share features of low-grade mucosal inflammation and epithelial barrier dysfunction.

The observed downregulation of TP53 by PRA warrants nuanced mechanistic consideration. While TP53 (p53) is canonically regarded as a tumor suppressor, within the context of intestinal epithelial stress responses, it functions as a central coordinator of cellular fate decisions following DNA damage, oxidative insult, and in-

flammatory injury. Under conditions of sustained low-grade inflammation—as typified by IBS-D—TP53 activation may paradoxically drive epithelial apoptosis and erode mucosal barrier integrity, thereby accelerating disease progression rather than conferring protection. The present finding that PRA reduced TP53 expression, concomitantly with the pro-apoptotic mediators Bax and cleaved caspase-3, while elevating the anti-apoptotic protein Bcl-2, implies that PRA may mitigate excessive stress-triggered apoptosis in intestinal epithelial cells, thus safeguarding mucosal homeostasis. This interpretation is congruent with the transcriptomic identification of CASP3 and TP53 as enriched core targets and substantiates the view that the anti-apoptotic actions of PRA represent an integral facet of its mucosal protective mechanism, rather than an incidental observation.

Furthermore, the current investigation demonstrated that both high-dose PRA and the RAGE antagonist FPS-ZM1 individually produced significant reductions in RAGE/NF-κB pathway molecule expression, while their co-administration yielded a more pronounced suppressive effect, indicating that the protective pharmacological actions of PRA are at least partly mediated through interference with the RAGE/NF-κB signaling axis. Prior investigations have shown that exogenous dietary advanced glycation end products can perturb gut microbial community structure and enhance colonic permeability [56,57,58], suggesting that subsequent studies could productively explore the interplay along the "AGE burden–microbiota–barrier" axis. Additionally, PRA administration decreased TP53, Bax, and cleaved-caspase-3 protein levels, increased Bcl-2 expression, and reduced TUNEL-positive cell counts, collectively indicating suppression of excessive distal colon tissue apoptosis. In the setting of intestinal mucosal injury, inflammation and apoptosis are recognized as mutually reinforcing processes: sustained inflammatory signaling can trigger epithelial cell death, and conversely, apoptotic loss of epithelial coverage further amplifies permeability increases and inflammatory spread. This mechanistic interconnection was independently corroborated by the transcriptomic enrichment of apoptosis-associated molecules, notably CASP3 and TP53. These observations are further supported by prior reports showing that natural polysaccharides can mend intestinal barrier injury and suppress NF-κB activation through gut microbiota modulation [59].

In synthesis, the following mechanistic model is proposed to account for the therapeutic actions of PRA in IBS-D: the multi-component bioactive arsenal of PRA may dampen AGE/RAGE/NF-κB signal transduction, thereby curtailing the release of downstream pro-inflammatory cytokines (IL-6, TNF-α, IL-1β, MCP-1, EDN1), which in sequence attenuates inflammatory amplification loops. In parallel, PRA may fortify epithelial barrier architecture by upregulating tight junction proteins (ZO-1, Occludin, Claudin-1) and the mucus barrier component MUC2, while simultaneously curbing excessive epithelial apoptosis through suppression of TP53, Bax, and cleaved caspase-3 and enhancement of Bcl-2 expression. Through these coordinated multi-level actions, PRA ultimately ameliorates the cardinal features of IBS-D, including diarrheal symptoms, mucosal tissue injury, and disordered intestinal motility. It must be emphasized that this model constitutes a working hypothesis derived from the present dataset, and additional functional validation experiments are required to establish definitive causal relationships.

5. Limitations

The additive therapeutic benefit observed when PRA was combined with the RAGE inhibitor FPS-ZM1 carries significant mechanistic implications. Were PRA to act exclusively via the AGE/RAGE axis, combined treatment would not be anticipated to surpass the maximal effect achievable with RAGE blockade alone. The synergistic improvement observed instead suggests that PRA likely engages pharmacological targets beyond the RAGE/NF-κB cascade, potentially encompassing direct free radical scavenging, gut microbiota community restructuring, and modulation of additional inflammatory signaling routes such as the MAPK and NLRP3 pathways. This interpretation is consistent with the inherent multi-component nature of PRA as a botanical medicine. The therapeutic efficacy of PRA is likely attributable to the concerted actions of multiple bioactive constituents—including paeoniflorin, benzoyl paeoniflorin, albiflorin, and kaempferol—rather than any single dominant compound. Indeed, prior investigations have established that paeoniflorin in isolation can counteract intestinal barrier disruption and quell LPS-provoked inflammatory responses in Caco-2 cell monolayers [21], and that PRA aqueous extract mitigates dextran sulfate sodium (DSS)-induced colitis through concurrent regulation of the intestinal physical barrier, immune function, and microbial community [22]. The present study extends this prior work by furnishing a systematic mechanistic framework that links PRA's multi-component chemical basis to the AGE/RAGE/NF-κB signaling axis through integrated transcriptomic and network pharmacology analysis. Moreover, recent progress in nanoparticulate drug delivery technologies has shown that natural product compounds can be engineered to improve their bioavailability and achieve targeted therapeutic delivery [60,61,62,63], presenting promising strategies for future optimization of PRA-derived interventions. In contrast to earlier investigations that examined individual compounds or isolated signaling pathways, the current work delivers genuine mechanistic advances by coupling multi-omics analytical approaches with experimental validation, yielding a more holistic understanding of PRA's therapeutic mode of action in IBS-D.

Although PRA's mechanism of action in IBS-D was systematically probed in this study, several caveats warrant acknowledgment. First, IBS-D patients display consider-

able pathological heterogeneity; while the animal model recapitulated certain features diarrhea, low-grade inflammation, and barrier impairment it could not fully capture the complexity of the human gut-brain axis, psychological stress dimensions, or individual patient variability. Second, although multiple core bioactive components and pivotal targets were identified, direct causal relationships between specific compounds and their predicted targets were not validated through single-compound intervention, gene knockout, or overexpression studies. Future investigations should integrate clinical specimens, multi-omics data integration, and functional experimental validation to more definitively map the active components, direct targets, and mechanistic pathways of PRA in IBS-D. Third, this study employed only male mice, potentially overlooking gender-specific differences in IBS-D pathophysiology and pharmacological response. Fourth, the PRA intervention period was limited to 14 days, leaving the long-term efficacy and safety profile of PRA in IBS-D unevaluated. Fifth, the current analysis centered on the AGE/RAGE/NF-κB pathway, and additional signaling cascades including MAPK, NLRP3 inflammasome, and gut microbiota-mediated mechanisms merit further exploration. Sixth, molecular-level dose-response characterization was not conducted for the low and medium PRA doses, constraining the understanding of PRA's optimal therapeutic dosing window. Seventh, the transcriptomic and network pharmacology approaches used here are inherently predictive, and the identified core targets and pathways necessitate further functional validation. Eighth, several important dimensions of IBS-D pathobiology, including gut microbiota shifts, visceral hypersensitivity, and neuroimmune signaling were not assessed in the present study, despite their increasingly recognized contributions to the disease. Ninth, the therapeutic intervention was initiated following model establishment, approximating a treatment rather than prevention paradigm; however, the 14-day duration constrains conclusions regarding sustained efficacy. Tenth, the translational gap between murine models and human IBS-D patients remains to be bridged, and well-designed clinical studies are essential to validate the therapeutic potential of PRA.

6. Conclusions

PRA was able to significantly improve the general condition of IBS-D model mice, alleviate intestinal mucosal pathological injury, restore the intestinal mucus barrier, reduce the levels of pro-inflammatory cytokines, and inhibit apoptosis in distal colon tissue. These findings suggest that PRA may exert beneficial effects partly through modulation of the AGE/RAGE/NF-κB pathway.

Availability of Data and Materials

All data generated or analyzed during this study are available from the corresponding author on reasonable request.

Author Contributions

Writing—original draft, PH, YY, FW, WW and JZ; writing—review and editing, PH, YY, FW, WW and JZ; supervision, PH; project administration, JZ; data collection, YY and FW; data analysis, WW; conducting experiments, PH and JZ. All authors read and approved the final manuscript. All authors have participated sufficiently in the work and agreed to be accountable for all aspects of the work.

Ethics Approval and Consent to Participate

Animal Experiment Ethics Committee of Heilongjiang University of Chinese Medicine (SYXK-202605012). All animal experiments were conducted in accordance with the revised UK Animals (Scientific Procedures) Act 1986. All animal experimental procedures were conducted in accordance with the principles of the 3Rs (Replacement, Reduction, and Refinement), and the study was reported following the ARRIVE guidelines for animal research.

Acknowledgment

Not applicable.

Funding

This research received no external funding.

Conflicts of Interest

The authors declare no conflicts of interest.

Supplementary Material

Supplementary material associated with this article can be found, in the online version, at https://doi.org/10.31083/IJP54720.

References

[1] Sebastián Domingo JJ. Irritable bowel syndrome. Medicina Clinica. 2022; 158: 76–81. https://doi.org/10.1016/j.medcli.2021.04.029 (In Spanish)

[2] Huang KY, Wang FY, Lv M, Ma XX, Tang XD, Lv L. Irritable bowel syndrome: Epidemiology, overlap disorders, pathophysiology and treatment. World Journal of Gastroenterology. 2023; 29: 4120–4135. https://doi.org/10.3748/wjg.v29.i26.4120

[3] Galica AN, Galica R, Dumitrașcu DL. Diet, fibers, and probiotics for irritable bowel syndrome. Journal of Medicine and Life. 2022; 15: 174–179. https://doi.org/10.25122/jml-2022-0028

[4] Altomare A, Di Rosa C, Imperia E, Emerenziani S, Cicala M, Guarino MPL. Diarrhea Predominant-Irritable Bowel Syndrome (IBS-D): Effects of Different Nutritional Patterns on Intestinal Dysbiosis and Symptoms. Nutrients. 2021; 13: 1506. https://doi.org/10.3390/nu13051506

[5] Sayuk GS. Medical Therapies for Diarrhea-Predominant Irritable Bowel Syndrome. Gastroenterology Clinics of North America. 2021; 50: 611–637. https://doi.org/10.1016/j.gtc.2021.04.003

[6] Martoni CJ, Srivastava S, Damholt A, Leyer GJ. Efficacy and dose response of Lactiplantibacillus plantarum in diarrhea-predominant irritable bowel syndrome. World Journal of Gastroenterology. 2023; 29: 4451–4465. https://doi.org/10.3748/wjg.v29.i28.4451
[7] Van Rooyen DM, Cai M, Nair BR, Talley NJ. Irritable bowel syndrome in the elderly: epidemiology, diagnosis, treatment, and relationship with frailty. Expert Review of Gastroenterology & Hepatology. 2026; 20: 381–394. https://doi.org/10.1080/17474124.2026.2651944
[8] Singh P, Nee J. Role of Diet in Diarrhea-predominant Irritable Bowel Syndrome. Journal of Clinical Gastroenterology. 2021; 55: 25–29. https://doi.org/10.1097/MCG.0000000000001445
[9] Mozaffari S, Nikfar S, Abdollahi M. Drugs of the future for diarrhea-predominant irritable bowel syndrome: an overview of current investigational drugs. Expert Opinion on Investigational Drugs. 2024; 33: 219–228. https://doi.org/10.1080/13543784.2024.2320703
[10] Munjal A, Dedania B, Cash BD. Current and emerging pharmacological approaches for treating diarrhea-predominant irritable bowel syndrome. Expert Opinion on Pharmacotherapy. 2020; 21: 63–71. https://doi.org/10.1080/14656566.2019.1691524
[11] Zheng H, Chen Y, Lu S, Liu Z, Ma Y, Zhang C, et al. Mechanosensory Piezo2 regulated by gut microbiota participates in the development of visceral hypersensitivity and intestinal dysmotility. Gut Microbes. 2025; 17: 2497399. https://doi.org/10.1080/19490976.2025.2497399
[12] Tomita T, Fukui H, Morishita D, Maeda A, Makizaki Y, Tanaka Y, et al. Diarrhea-predominant Irritable Bowel Syndrome-like Symptoms in Patients With Quiescent Crohn's Disease: Comprehensive Analysis of Clinical Features and Intestinal Environment Including the Gut Microbiome, Organic Acids, and Intestinal Permeability. Journal of Neurogastroenterology and Motility. 2023; 29: 102–112. https://doi.org/10.5056/jnm22027
[13] Bai X, Ihara E, Tanaka Y, Minoda Y, Wada M, Hata Y, et al. The interplay of gut microbiota and intestinal motility in gastrointestinal function. Journal of Smooth Muscle Research = Nihon Heikatsukin Gakkai Kikanshi. 2025; 61: 51–58. https://doi.org/10.1540/jsmr.61.51
[14] Kułak-Bejda A, Bejda G, Waszkiewicz N. Antidepressants for irritable bowel syndrome-A systematic review. Pharmacological Reports: PR. 2017; 69: 1366–1379. https://doi.org/10.1016/j.pharep.2017.05.014
[15] Weber HC. New treatment options for irritable bowel syndrome with predominant diarrhea. Current Opinion in Endocrinology, Diabetes, and Obesity. 2017; 24: 25–30. https://doi.org/10.1097/MED.0000000000000302
[16] Bassotti G. Targeting diarrhea-predominant irritable bowel syndrome: hopes or hypes? Expert Opinion on Investigational Drugs. 2025; 34: 459–462. https://doi.org/10.1080/13543784.2024.2347296
[17] Huang B, An H, Qiu Y, Ye T, Huang Y, Zheng M, et al. Comparative Effectiveness and Safety of Fecal Microbiota Transplantation in Ulcerative Colitis: An Updated Systematic Review and Meta-Analysis. Advances in Therapy. 2026; 43: 2645–2667. https://doi.org/10.1007/s12325-025-03431-0
[18] Mu X, Luan R, Gao Y, Zhao B, Wang J, Ni X, et al. The Traditional Applications, Phytochemistry, Pharmacology, Pharmacokinetics, Quality Control and Safety of Paeoniae Radix Alba: A Review. The American Journal of Chinese Medicine. 2024; 52: 2337–2376. https://doi.org/10.1142/S0192415X24500897
[19] Wang YR, Gao YQ, Liu ZL, Liu W, Cui WQ, Wu HY, et al. Paeoniflorin as a potential therapeutic agent for cerebrovascular diseases: A comprehensive review. Pharmacological Research. 2025; 221: 107965. https://doi.org/10.1016/j.phrs.2025.107965
[20] Yan B, Shen M, Fang J, Wei D, Qin L. Advancement in the chemical analysis of Paeoniae Radix (Shaoyao). Journal of Pharmaceutical and Biomedical Analysis. 2018; 160: 276–288. https://doi.org/10.1016/j.jpba.2018.08.009
[21] Wu XX, Huang XL, Chen RR, Li T, Ye HJ, Xie W, et al. Paeoniflorin Prevents Intestinal Barrier Disruption and Inhibits Lipopolysaccharide (LPS)-Induced Inflammation in Caco-2 Cell Monolayers. Inflammation. 2019; 42: 2215–2225. https://doi.org/10.1007/s10753-019-01085-z
[22] Yan BF, Chen X, Chen YF, Liu SJ, Xu CX, Chen L, et al. Aqueous extract of Paeoniae Radix Alba (Paeonia lactiflora Pall.) ameliorates DSS-induced colitis in mice by tunning the intestinal physical barrier, immune responses, and microbiota. Journal of Ethnopharmacology. 2022; 294: 115365. https://doi.org/10.1016/j.jep.2022.115365
[23] Hou Y, Luo F, Wang K, Chen Y, Wang L, Li Y, et al. Electroacupuncture restores intestinal mucosal barrier in IBS-D rats by modulating mast cell-derived exosomal MiR-149-5p. Frontiers in Immunology. 2025; 16: 1641484. https://doi.org/10.3389/fimmu.2025.1641484
[24] Percie du Sert N, Hurst V, Ahluwalia A, Alam S, Avey MT, Baker M, et al. The ARRIVE guidelines 2.0: Updated guidelines for reporting animal research. PLoS Biology. 2020; 18: e3000410. https://doi.org/10.1371/journal.pbio.3000410
[25] Drossman DA, Hasler WL. Rome IV-Functional GI Disorders: Disorders of Gut-Brain Interaction. Gastroenterology. 2016; 150: 1257–1261. https://doi.org/10.1053/j.gastro.2016.03.035
[26] Chey WD, Kurlander J, Eswaran S. Irritable bowel syndrome: a clinical review. JAMA. 2015; 313: 949–958. https://doi.org/10.1001/jama.2015.0954
[27] Enck P, Aziz Q, Barbara G, Farmer AD, Fukudo S, Mayer EA, et al. Irritable bowel syndrome. Nature Reviews. Disease Primers. 2016; 2: 16014. https://doi.org/10.1038/nrdp.2016.14
[28] Walker JR, Ediger JP, Graff LA, Greenfeld JM, Clara I, Lix L, et al. The Manitoba IBD cohort study: a population-based study of the prevalence of lifetime and 12-month anxiety and mood disorders. The American Journal of Gastroenterology. 2008; 103: 1989–1997. https://doi.org/10.1111/j.1572-0241.2008.01980.x
[29] Xiao L, Liu Q, Luo M, Xiong L. Gut Microbiota-Derived Metabolites in Irritable Bowel Syndrome. Frontiers in Cellular and Infection Microbiology. 2021; 11: 729346. https://doi.org/10.3389/fcimb.2021.729346
[30] Body-Malapel M, Djouina M, Waxin C, Langlois A, Gower-Rousseau C, Zerbib P, et al. The RAGE signaling pathway is involved in intestinal inflammation and represents a promising therapeutic target for Inflammatory Bowel Diseases. Mucosal Immunology. 2019; 12: 468–478. https://doi.org/10.1038/s41385-018-0119-z
[31] Shen CY, Lu CH, Wu CH, Li KJ, Kuo YM, Hsieh SC, et al. The Development of Maillard Reaction, and Advanced Glycation End Product (AGE)-Receptor for AGE (RAGE) Signaling Inhibitors as Novel Therapeutic Strategies for Patients with AGE-Related Diseases. Molecules (Basel, Switzerland). 2020; 25: 5591. https://doi.org/10.3390/molecules25235591
[32] Snelson M, Lucut E, Coughlan MT. The role of AGE-RAGE signalling as a modulator of gut permeability in diabetes. International Journal of Molecular Sciences. 2022; 23: 1766. https://doi.org/10.3390/ijms23031766
[33] Li Z, Zhao Z, Chen S, Wang X, Wang D, Nie X, et al. Ge-Gen-Qin-Lian decoction alleviates the symptoms of type 2 diabetes mellitus with inflammatory bowel disease via regulating the AGE-RAGE pathway. BMC Complementary Medicine and Therapies. 2024; 24: 225. https://doi.org/10.

1186/s12906-024-04526-x
[34] Prasad K, Mishra M. AGE-RAGE Stress, Stressors, and Antistressors in Health and Disease. The International Journal of Angiology: Official Publication of the International College of Angiology, Inc. 2018; 27: 1–12. https://doi.org/10.1055/s-0037-1613678
[35] Chen Q, Zhang H, Sun CY, He QY, Zhang RR, Luo BF, et al. Evaluation of two laboratory model methods for diarrheal irritable bowel syndrome. Molecular Medicine (Cambridge, Mass.). 2023; 29: 5. https://doi.org/10.1186/s10020-022-00599-x
[36] Wells JM, Brummer RJ, Derrien M, MacDonald TT, Troost F, Cani PD, et al. Homeostasis of the gut barrier and potential biomarkers. American Journal of Physiology. Gastrointestinal and Liver Physiology. 2017; 312: G171–G193. https://doi.org/10.1152/ajpgi.00048.2015
[37] Takiishi T, Fenero CIM, Câmara NOS. Intestinal barrier and gut microbiota: Shaping our immune responses throughout life. Tissue Barriers. 2017; 5: e1373208. https://doi.org/10.1080/21688370.2017.1373208
[38] Yan S, Xie Y, Xv J, Wang K, Wang J, Cao Y, et al. Shengjiang San attenuates sepsis-induced acute intestinal injury via Lactobacillus murinus derived IAAld-mediated macrophage polarization through NF-κB and TGF-β signaling. Journal of Ethnopharmacology. 2026; 357: 120910. https://doi.org/10.1016/j.jep.2025.120910
[39] Ming L, Ji J, Luo Z, Zhao Z, Li M, Sun R, et al. Sishen pill alleviates DSS induced colitis through AGE/RAGE/NLRP3 pathway based on transcriptomics analysis. Journal of Ethnopharmacology. 2026; 356: 120818. https://doi.org/10.1016/j.jep.2025.120818
[40] Jiang W, Yin J, Han M, He W, Zhao Y, Hu J, et al. N4BP3 Activates TLR4-NF-κB Pathway in Inflammatory Bowel Disease by Promoting K48-Linked IκBα Ubiquitination. Journal of Inflammation Research. 2025; 18: 7167–7181. https://doi.org/10.2147/JIR.S518155
[41] Huang B, An H, Chen L, Lin H, Wu H, Li R, et al. Comparative efficacy and safety of mesalazine-based regimens with traditional Chinese medicines in mild-to-moderate ulcerative colitis. Frontiers in Pharmacology. 2026; 16: 1691460. https://doi.org/10.3389/fphar.2025.1691460
[42] Wu H, Zhan K, Rao K, Zheng H, Qin S, Tang X, et al. Comparison of five diarrhea-predominant irritable bowel syndrome (IBS-D) rat models in the brain-gut-microbiota axis. Biomedicine & Pharmacotherapy = Biomedecine & Pharmacotherapie. 2022; 149: 112811. https://doi.org/10.1016/j.biopha.2022.112811
[43] He YQ, Zhu JR, Sun WJ, Luo YY, Wu XF, Yang M, et al. ZO-1 and IL-1RAP Phosphorylation: Potential Role in Mediated Brain-Gut Axis Dysregulation in Irritable Bowel Syndrome-like Stressed Mice. International Journal of Medical Sciences. 2024; 21: 1738–1755. https://doi.org/10.7150/ijms.95848
[44] Zhang S, Tian D, Xia Z, Yang F, Chen Y, Yao Z, et al. Chang-Kang-Fang alleviates diarrhea predominant irritable bowel syndrome (IBS-D) through inhibiting TLR4/NF-κB/NLRP3 pathway. Journal of Ethnopharmacology. 2024; 330: 118236. https://doi.org/10.1016/j.jep.2024.118236
[45] Zhang MM, Dang M, Wu X, Ou L, Li M, Zhao CB, et al. Da-Jian-Zhong decoction alleviates diarrhea-predominant irritable bowel syndrome via modulation of gut microbiota and Th17/Treg balance. Journal of Ethnopharmacology. 2024; 331: 118275. https://doi.org/10.1016/j.jep.2024.118275
[46] Ma Q, Jiang Z, Zhang Z, Sun L, Su T, Liu Z, et al. Qizhiweitong granule alleviates diarrhea-predominant irritable bowel syndrome via inhibition of the IL-6/Src/STAT3 feedback loop. Journal of Ethnopharmacology. 2026; 356: 120772. https://doi.org/10.1016/j.jep.2025.120772
[47] Lin H, Lv Y, Liu H, Lin Z, Zhu N, Huang B. Baicalein alleviates chronic acute stress-induced irritable bowel syndrome-like symptoms in rats via modulating the ODC1/NF-κB pathway and oxidative stress. Biochemical and Biophysical Research Communications. 2025; 771: 152058. https://doi.org/10.1016/j.bbrc.2025.152058
[48] Chen X, Chen C, Ma C, Kang W, Wu J, Fu X. Dendrobium officinale polysaccharide attenuates type 2 diabetes in mice model by modulating gut microbiota and alleviating intestinal mucosal barrier damage. Food Science and Human Wellness. 2025; 14: 9250007. https://doi.org/10.26599/fshw.2024.9250007
[49] Zhang C, Li H, Xu M, Pu C, Zhu Y, Du L, et al. Remodeling the gut ecosystem and its mechanism: Natural products in the treatment of ulcerative colitis via regulating gut microbiota and metabolites. International Immunopharmacology. 2026; 174: 116378. https://doi.org/10.1016/j.intimp.2026.116378
[50] Yan SF, Ramasamy R, Schmidt AM. Soluble RAGE: Therapy and biomarker in unraveling the RAGE axis in chronic disease and aging. Biochemical Pharmacology. 2010; 79: 1379–1386. https://doi.org/10.1016/j.bcp.2010.01.013
[51] Hagiwara S, Sourris K, Ziemann M, Tieqiao W, Mohan M, McClelland AD, et al. RAGE Deletion Confers Renoprotection by Reducing Responsiveness to Transforming Growth Factor-β and Increasing Resistance to Apoptosis. Diabetes. 2018; 67: 960–973. https://doi.org/10.2337/db17-0538
[52] Zhou Q, Lei L, Cheng J, Chen J, Du Y, Zhang X, et al. Microbiota-induced S100A11-RAGE axis underlies immune evasion in right-sided colon adenomas and is a therapeutic target to boost anti-PD1 efficacy. Gut. 2025; 74: 214–228. https://doi.org/10.1136/gutjnl-2024-332193
[53] Cho E, Mun SJ, Kim HK, Ham YS, Gil WJ, Yang CS. Colon-targeted S100A8/A9-specific peptide systems ameliorate colitis and colitis-associated colorectal cancer in mouse models. Acta Pharmacologica Sinica. 2024; 45: 581–593. https://doi.org/10.1038/s41401-023-01188-2
[54] Raman KG, Sappington PL, Yang R, Levy RM, Prince JM, Liu S, et al. The role of RAGE in the pathogenesis of intestinal barrier dysfunction after hemorrhagic shock. American Journal of Physiology-Gastrointestinal and Liver Physiology. 2006; 291: G556–G565. https://doi.org/10.1152/ajpgi.00055.2006
[55] Febrinasari RP, Indah SP, Bastomy ER, Irving S, Azmiardi A, Pribadi RR, et al. A systematic review and meta-analysis of the relationship between advanced glycation end products ceceptor (RAGE) gene polymorphisms and the risk of inflammatory bowel disease. Caspian Journal of Internal Medicine. 2023; 14: 412–424. https://doi.org/10.22088/cjim.14.3.41
[56] Cho CH, Jung YS, Kim M, Kurniawati UD, Kim Y, Yim MJ, et al. Modulating intestinal health: Impact of chitooligosaccharide molecular weight on suppressing RAGE expression and inflammatory response in methylglyoxal-induced advanced glycation end-products. International Journal of Biological Macromolecules. 2024; 269: 131927. https://doi.org/10.1016/j.ijbiomac.2024.131927
[57] Chen YY, Chen SY, Chang HY, Liu YC, Chuang BF, Yen GC. Phyllanthus emblica L. polysaccharides ameliorate colitis via microbiota modulation and dual inhibition of the RAGE/NF-κB and MAPKs signaling pathways in rats. International Journal of Biological Macromolecules. 2024; 258: 129043. https://doi.org/10.1016/j.ijbiomac.2023.129043
[58] Yuan X, Liu J, Nie C, Ma Q, Wang C, Liu H, et al. Comparative Study of the Effects of Dietary-Free and -Bound Nε-Carboxymethyllysine on Gut Microbiota and Intestinal Barrier. Journal of Agricultural and Food Chemistry. 2024; 72: 5014–5025. https://doi.org/10.1021/acs.jafc.3c09395

[59] Chen X, Chen C, Fu X. Dendrobium officinale Polysaccharide Alleviates Type 2 Diabetes Mellitus by Restoring Gut Microbiota and Repairing Intestinal Barrier via the LPS/TLR4/TRIF/NF-kB Axis. Journal of Agricultural and Food Chemistry. 2023; 71: 11929–11940. https://doi.org/10.1021/acs.jafc.3c02429

[60] Tarin M, Oryani MA, Javid H, Tajaldini M, Hashemzadeh A, Karimi-Shahri M. Synergistic engineering of pH-responsive MSN@ZIF-8 core-shell nanohybrids for targeted cancer therapy: from rational design to clinical potential. Nanotechnology. 2026; 37: 232005. https://doi.org/10.1088/1361-6528/ae6f1e

[61] Sajjadi SS, Einafshar E, Javid H, Assaran Darban R, Jafari N, Hashemy SI. Chitosan-embedded β-cyclodextrin-magnetic graphene oxide nanoparticles for curcumin loading: evaluating cytotoxicity and apoptosis induction in esophageal cancer. Naunyn-Schmiedeberg's Archives of Pharmacology. 2026; 399: 4357–4369. https://doi.org/10.1007/s00210-025-04737-0

[62] Einafshar E, Jafarzadeh T, Javid H, Amiri H, Hosseini H. Enhancement of the protective effect of diosmin against glutamate-induced toxicity by selenium-chitosan nanoparticle formulation. Journal of Nanoparticle Research. 2025; 27: 265. https://doi.org/10.1007/s11051-025-06462-4

[63] Tong Q, Yang Y, Xiong Z, Li Z, Yuan W, Wang T. Chitooligosaccharides downregulate TLR4/NF-κB/COX-2 signaling cascade in dextran sulfate sodium-treated mice: a potential mechanism for the anti-colitis effect. International Journal of Pharmacology. 2016; 12: 720–728.